NACA TN 3410

NATIONAL ADVISORY COMMITTEE FOR AERONAUTICS

TECHNICAL NOTE 3410

VARIATION OF LOCAL LIQUID-WATER CONCENTRATION ABOUT AN ELLIPSOID OF FINENESS RATIO 10 MOVING IN A DROPLET FIELD

By Rinaldo J. Brun and Robert G. Dorsch

Lewis Flight Propulsion Laboratory
Cleveland, Ohio

Washington
April 1955

NATIONAL ADVISORY COMMITTEE FOR AERONAUTICS

TECHNICAL NOTE 3410

VARIATION OF LOCAL LIQUID-WATER CONCENTRATION ABOUT AN ELLIPSOID OF FINENESS RATIO 10 MOVING IN A DROPLET FIELD

By Rinaldo J. Brun and Robert G. Dorsch

SUMMARY

Trajectories of water droplets about an ellipsoid of revolution with a fineness ratio of 10 (10 percent thick) in flight through a droplet field were computed with the aid of a differential analyzer. Analyses of these trajectories indicate that the local concentration of liquid water at various points about an ellipsoid varies considerably and under some conditions may be several times the free-stream concentration. Curves of the local concentration factor as a function of spatial position were obtained and are presented in terms of dimensionless parameters that describe flight and atmospheric conditions. The data indicate that the expected local concentration factors should be considered when choosing the location of devices that protrude into the stream from aircraft fuselages or missiles, or when determining anti-icing heat requirements for the protection of these devices.

INTRODUCTION

The calculations presented herein were made in order to extend the study reported in reference 1 on the spatial distribution of cloud droplet concentration after the free-stream concentration and distribution are altered by an aerodynamic body moving through the cloud. In reference 1 the alteration of the concentration of cloud droplets in the immediate vicinity of an ellipsoid of revolution with a fineness ratio of 5 (20 percent thick) is discussed; whereas, the data herein apply to an ellipsoid with a fineness ratio of 10 (10 percent thick).

As is discussed in the reference cited, an aircraft moving through a cloud alters the concentration of cloud droplets in the immediate vicinity of the aircraft. During flight in supercooled clouds, an uneven distribution of ice is often formed on rod-shaped objects that protrude from the fuselage. An illustration of this peculiar distribution is shown in photographs presented in reference 1 and in figure 1 of this report. The pitot mast shown in figure 1 was attached to the fuselage of a B-24 airplane. As indicated by this ice formation, there

is frequently a region of reduced (or zero) droplet concentration next to the aircraft surface, followed by a narrow region of greatly increased droplet concentration farther out. Beyond the narrow region of high concentration, the droplet concentration gradually decreases toward the free-stream value with increase in distance from the surface of the aircraft. A sketch of a typical spatial variation is shown in figure 2.

A knowledge of this spatial variation of local droplet concentration about an aircraft or missile during flight through clouds, drizzle, or rain is often important when choosing the location of devices that protrude into the stream or when determining the design requirements for icing protection on the devices. Examples of such devices are: (1) intake ducts and vents, (2) antenna masts, (3) ice detectors, and (4) instruments for measuring liquid-water content and droplet-size distribution. Similarly, at places where a body of revolution joins an airfoil (i.e., where there is a forebody ahead of the airfoil, such as a rocket pod or aircraft fuselage), the local impingement of cloud droplets on the airfoil, and therefore the ice-protection design requirements, will be altered by the effect of the body of revolution on the local droplet concentration.

The nonuniform distribution of ice shown in figures 1 and 2 can be explained from a knowledge of the trajectories of cloud droplets around the fuselage. Droplet trajectories about an ellipsoid of fineness ratio of 10 (10 percent thick) in axisymmetric, incompressible flow were calculated with the aid of a differential analyzer at the NACA Lewis laboratory. A prolate ellipsoid is chosen as a good approximation for many fuselages and missile bodies, and has the additional advantage of a surrounding flow field that is known exactly for incompressible, nonviscous flow. A knowledge of the flow field is necessary for the computation of the droplet trajectories, which were calculated back to the midpoint of the ellipsoid and in space in the radial direction as far out as a distance equal to the minor axis. These trajectories were analyzed to determine the relation between the droplet concentration at various points in space with the following variables: ellipsoid length and velocity, droplet size, flight altitude, and air temperature. The results of the analysis are summarized in this report in terms of the dimensionless parameters Re_0 and K, which include these variables. Although the calculations were made for incompressible flow, they should be applicable throughout the subsonic region because of the small effect of compressibility on droplet trajectories (ref. 2) and because of the high flight critical Mach number of the ellipsoid.

SYMBOLS

The following symbols are used in this report:

A	annular area perpendicular to major axis through which droplet flux flows, sq ft
C	local concentration factor, $d(r_0^2)/d(r^2)$, dimensionless
d	droplet diameter, microns
F	flux density of liquid water, lb/(hr)(sq ft)
K	inertia parameter, $1.704 \times 10^{-12} d^2 U/\mu L$, dimensionless (density of water, 1.94 slugs/cu ft, is included in constant)
L	length of ellipsoid major axis, ft
Re_0	free-stream Reynolds number with respect to droplet diameter $4.813 \times 10^{-6} d \rho_a U/\mu$, dimensionless
$Re_{0,med}$	free-stream Reynolds number based on volume-median droplet diameter, dimensionless
r,z	cylinder coordinates, ratio to major axis, dimensionless (fig. 3)
r_0	starting ordinate at $z = -\infty$ of droplet trajectory, ratio to major axis, dimensionless
U	free-stream velocity or flight speed, mph
u	ratio of local air velocity to free-stream velocity, dimensionless
v'	local droplet velocity, mph
w	local liquid-water content, g/cu m
μ	viscosity of air, slugs/(ft)(sec)
ρ_a	density of air, slugs/cu ft

Subscripts:

av	average of quantity over area A
r	radial component
s	ellipsoid surface
z	axial component
0	free-stream conditions

METHOD OF COMPUTING DROPLET TRAJECTORIES

The equations that describe the motion of cloud droplets about an ellipsoid are given in reference 3. A solution of the differential equations of motion was obtained with the use of a mechanical analog (described in ref. 4) based on the principle of a differential analyzer. The procedure for calculating the trajectories of cloud droplets with respect to the ellipsoid is the same as that described in references 1, 3, and 5. As shown in figure 3, the ellipsoid orientation in the coordinate system used in references 1, 3, and 5 is retained herein. Since a flow field is axisymmetric around an ellipsoid of revolution oriented at 0° between its major axis and the direction of the free stream, the droplet trajectories in the elliptical section of all meridian planes are the same, and the spatial variation of concentration can be obtained from trajectory calculations in the z,r plane of figure 3.

The equations describing the air-flow field around the body, required for the solution of the equations of droplet motion, are given in reference 3. The values of the air-velocity components u_z and u_r as functions of r and z are given graphically in reference 5.

RESULTS AND DISCUSSION OF TRAJECTORY COMPUTATIONS

Dimensionless Parameters

The equations of motion were solved for various values of the parameter $1/K$ between 0.1 and 90. The inertial parameter K is a measure of the droplet size, the flight speed and size of the body of revolution, and the viscosity of the air, in the form

$$K = 1.704 \times 10^{-12} \frac{d^2 U}{\mu L} \tag{1}$$

The density of water, which is expressed as part of the conversion factor, is 1.94 slugs per cubic foot. For each value of the parameter $1/K$, a series of trajectories was computed for each of several values of free-stream Reynolds number Re_0. The free-stream Reynolds number is defined with respect to the droplet diameter as

$$Re_0 = 4.813 \times 10^{-6} d\rho_a U/\mu \tag{2}$$

In order to make these dimensionless parameters more physically significant in the following discussion, some typical combinations of K and Re_0 are presented in table I for various lengths and velocities of the ellipsoid, droplet sizes, and flight pressure altitudes and

temperatures. A procedure for rapid calculation of $1/K$ and Re_0 from practical flight conditions is given in appendix B of reference 6.

Average Mass Flux Density of Water in Droplet Form

The average mass flux of water in droplet form per unit area through an annular area of space (of width $r_2 - r_1$, fig. 3) perpendicular to the major axis of the ellipsoid is obtained from the law of conservation of matter. Assume that the liquid water in droplet form is moving between two surfaces formed by rotating two neighboring trajectories in the r,z plane about the axis of the ellipsoid, as shown in figure 3. Then,

$$w_0 U A_0 = w_{av}\, v'_{z,av}\, A \tag{3}$$

and

$$\frac{F_{av}}{F_0} = \frac{w_{av} v'_{z,av}}{w_0 U} = \frac{A_0}{A} = \frac{r_{0,2}^2 - r_{0,1}^2}{r_2^2 - r_1^2} = \frac{\Delta(r_0^2)}{\Delta(r^2)} \tag{4}$$

The subscript 0 refers to conditions at large distances ahead of the ellipsoid (free-stream conditions), and the subscript av refers to the average of a quantity over the annular area A. The annular area A is measured in a plane perpendicular to the major axis of the ellipsoid (fig. 3). From equation (4), the average flux density through an annular area A or a sector of the annular area A can be written as follows:

$$F_{av} = 0.33 w_0 U \frac{\Delta(r_0^2)}{\Delta(r^2)},\ \text{lb/(hr)(sq ft)} \tag{5}$$

The constant 0.33 is a conversion factor for the units used.

Curves of r_0^2 as a function of r^2 are presented in figure 4 for various values of Re_0 and $1/K$ at three constant z-positions, the midpoint ($z = 0$), a point 1/4 major axis length from the noze ($z = -0.25$), and the tip of the nose ($z = -0.5$). These curves were obtained from calculated droplet trajectories. Equation (5) and figure 4 may be used, for example, to determine the amount of water in droplet form passing in a spatial region of cross-sectional annular area A located outside the ellipsoid a distance r from the major axis.

Local Liquid-Water Flux Density

The local mass flux of water in droplet form per unit area perpendicular to the major axis at a point in the vicinity of the moving ellipsoid can be obtained from equation (5) by letting $\Delta(r^2)$ approach zero as a limit. Then

$$F = 0.33 w_0 UC, \text{ lb/(hr)(sq ft)} \tag{6}$$

where

$$C = d(r_0^2)/d(r^2)$$

The local concentration factor C at a point in space is obtained from the slope of the curves of r_0^2 as a function of r^2 (fig. 4) at the point of interest for the Re_0 and K combination being considered.

The concentration factor C as a function of r for selected values of Re_0 and K at $z = 0$, -0.25, and -0.5 is given in figure 5. As was stated for the 20-percent-thick ellipsoid in reference 1, the concentration factor approaches 1 (free-stream value) at large values of r for all z-positions. As in the case of the 20-percent-thick ellipsoid, the concentration factor is less than the free-stream value ($C < 1$) at the nose of the ellipsoid ($z = -0.50$) near the major axis (small values of r, fig. 5(m)). At $z = -0.50$ no difference was found, within the accuracy of the computation, when Re_0 was changed and the value of $1/K$ was retained.

The peak values of the concentration factor given in figure 5 are plotted in figure 6 as a function of $1/K$ for various values of Re_0. The peak values are given only for the midpoint ($z = 0$) and the quarter point ($z = -0.25$) on the ellipsoid, because peak values do not exist at the nose ($z = -0.50$). The peak values of C were not well established by the trajectory computations for all values of Re_0 and $1/K$. For some cases, such as those given in figure 5(b), the peak values might be 50 percent higher than shown. The values shown in figures 5 and 6 are weighted for consistency with other data available on this subject, including the data of reference 1.

The r-position of the peak value of C at $z = 0$ and $z = -0.25$ is plotted as a function of $1/K$ for constant Re_0 in figure 7. With the use of figures 6 and 7, the peak value of C and its r position can be determined for the value of Re_0 and $1/K$ of interest.

The local liquid-water content in grams per cubic meter can be obtained at any point in space by dividing the droplet flux by the z-component of the local droplet velocity at that point:

$$w = \frac{w_0 U}{v_z'} C, \text{ g/cu m} \tag{7}$$

The value of the z-component of the droplet velocity v_z' was noted during the calculations of the droplet trajectories. A value of $v_z'/U \simeq 1$ (±1 percent) was observed between $z = -0.40$ and $z = 0$. A value of $v_z'/U \simeq 0.98$ (±2 percent) was observed between $z = -0.50$ and $z = -0.40$.

Shadow Zone

The region of zero concentration adjacent to the surface of the ellipsoid, which is illustrated in figure 2 and is evident in figure 5, is called the shadow zone. This region is protected from droplet penetration by the air-flow characteristics ahead of and in the vicinity of the forward positions of the ellipsoid. The thickness $(r - r_s)$ of the shadow zone at each z-position of the body for various Re_0 and K values is given in figure 8. Generally, the thickness of the shadow zone increases as z approaches 0, that is, from nose to midpoint of the ellipsoid. The shadow zone is 0 at the nose for all values of Re_0 and $1/K$ shown in figure 8 and becomes of finite thickness at a z-position that depends on Re_0 and $1/K$.

Comparison of 10- and 20-Percent-Thick Ellipsoids

Because a complete comparison of the 10- and 20-percent-thick ellipsoids that covers a wide range of flight and atmospheric conditions is beyond the scope of this report, the following limited comparison is made for a set of conditions that occur rather frequently. However, a danger must be noted arising from the choice of only a few sets of conditions for comparison: the relative importance of the different factors being compared may change with other conditions not discussed.

As might be expected, the shapes of the curves for peak values of concentration factor C and for shadow zone (figs. 6 and 8, respectively) resemble the curves describing the same factors in reference 1 for the 20-percent-thick ellipsoid. The principal difference between the curves for the two ellipsoids is that the effect of concentration

and the extent of shadow are not as great for the 10-percent-thick ellipsoid as for the 20-percent-thick body. The effect of a change in body thickness on peak value of concentration factor C is shown in figure 9 for an ellipsoid 10 feet long moving at 300 miles per hour at 15,000 feet altitude through droplets 20 microns in diameter. The effect of change in body thickness on the shadow zone under the same conditions is shown in figure 10. The thin body deflects the droplet trajectories from straight lines less than the thick body. For a body of zero thickness, the concentration factor would equal the free-stream value everywhere in space and the shadow zone is eliminated.

The variation of local concentration factor with spatial position and Re_0 and $1/K$ is discussed in reference 1. The concentration factor is very sensitive to small changes in $1/K$ and Re_0, as can be seen in figure 5. The variation of concentration of liquid-water content with z- and r-position and $1/K$ and Re_0 indicates that care should also be exercised with the 10-percent-thick body in locating instrument sensing elements and small inlets or vents that protrude from the surface and are sensitive to impinging water or ice formation.

The values presented in figures 4 to 8 apply directly only to flights in clouds composed of droplets that are all uniform in size. The effect of droplet-size distribution on concentration factor is discussed in reference 1 with the use of several illustrative examples. The manner in which the concentration factor applicable to a 10-percent-thick ellipsoid is altered by droplet-size distribution is given here for the same conditions used in one of the illustrative examples in reference 1.

With the use of the same flight and atmospheric conditions, a comparison with the 20-percent-thick ellipsoid is possible, as shown in figure 11. The abscissa is the distance from the ellipsoid surface, in inches, at $z = 0$. For both the 10- and 20-percent-thick ellipsoids, the major axis length is 20 feet, the flight speed is 300 miles per hour, the altitude is 15,000 feet, and the volume-median droplet diameter is 20 microns. For both bodies the peak value of the concentration factor considerably decreases as the distribution broadens from uniform droplets to a "C" distribution (defined in ref. 1). Also, the region that was a former shadow zone with zero concentration for the cloud condition with uniform droplets becomes an area with a small concentration factor. A comparison of concentration-factor curves calculated for droplet-size distributions estimated to be present in clouds, such as shown in figure 11, shows good qualitative agreement with the shape of actual ice formations obtained on rod-shaped objects in flight through the clouds (fig. 1).

CONCLUDING REMARKS

The significance of the spatial variation of liquid-water content and droplet size is discussed thoroughly in reference 1. The effect of the spatial variation on measuring instruments and on the rotating multicylinder method is also evaluated in reference 1. The importance of avoiding measurements of liquid water and droplet size in the region of variation of droplet concentration in the vicinity of an aircraft fuselage is emphasized, because the correction of the indicated water content and droplet-size distributions to free-stream conditions would be very involved.

The data of this report are applicable in a quantitative manner only to ellipsoids of revolution with a fineness ratio of 10. As was stated in reference 1 for a thicker body (fineness ratio of 5), these data also apply approximately in the vicinity of the nose section of a body of revolution that can be physically matched with the nose section of a 10-percent-thick ellipsoid of a given length. The data are particularly applicable if the afterbody does not appreciably alter the air-flow field ahead of the ellipsoid section from that attendant to an ellipsoid. Because many bodies of revolution of interest are different in shape from an ellipsoid, the data of this report and reference 1 are primarily useful in pointing out in a qualitative manner the type of variation in liquid-water concentration that might be expected in the vicinity of a body of revolution in flight through a droplet field.

Lewis Flight Propulsion Laboratory
National Advisory Committee for Aeronautics
Cleveland, Ohio, February 1, 1955

REFERENCES

1. Dorsch, Robert G., and Brun, Rinaldo J.: Variation of Local Liquid-Water Concentration about an Ellipsoid of Fineness Ratio 5 Moving in a Droplet Field. NACA TN 3153, 1954.

2. Brun, Rinaldo J., Serafini, John S., and Gallagher, Helen M.: Impingement of Cloud Droplets on Aerodynamic Bodies as Affected by Compressibility of Air Flow Around the Body. NACA TN 2903, 1953.

3. Dorsch, Robert G., Brun, Rinaldo J., and Gregg, John L.: Impingement of Water Droplets on an Ellipsoid with Fineness Ratio 5 in Axisymmetric Flow. NACA TN 3099, 1954.

4. Brun, Rinaldo J., and Mergler, Harry W.: Impingement of Water Droplets on a Cylinder in an Incompressible Flow Field and Evaluation of Rotating Multicylinder Method for Measurement of Droplet-Size Distribution, Volume-Median Droplet Size, and Liquid-Water Content in Clouds. NACA TN 2904, 1953.

5. Brun, Rinaldo J., and Dorsch, Robert G.: Impingement of Water Droplets on an Ellipsoid with Fineness Ratio 10 in Axisymmetric Flow. NACA TN 3147, 1954.

6. Brun, Rinaldo J., Gallagher, Helen M., and Vogt, Dorothea E.: Impingement of Water Droplets on NACA 65_1-208 and 65_1-212 Airfoils at 4° Angle of Attack. NACA TN 2952, 1953.

TABLE I. - RELATION OF DIMENSIONLESS PARAMETERS TO ELLIPSOID SIZE AND ATMOSPHERIC AND FLIGHT CONDITIONS

Atmospheric condition	Ellipsoid velocity, U, mph	Droplet diameter, d, microns	Major axis, L, ft	Pressure altitude, ft: 5000			15,000			25,000		
				Temperature, °F: 20			1			-25		
				Re_0	K	1/K	Re_0	K	1/K	Re_0	K	1/K
Cloud droplets	50	10	3	14.7	0.008123	123.1	10.72	0.008383	119.3	7.836	0.008793	113.7
			30	14.7	.0008123	1231	10.72	.0008383	1193	7.836	.0008793	1137
			100	14.7	.0002437	4103	10.72	.0002515	3976	7.836	.0002638	3791
		50	3	73.54	0.2031	4.924	53.62	0.2096	4.771	39.17	0.2198	4.550
			30	73.54	.02031	49.24	53.62	.02096	47.71	39.17	.02198	45.50
			100	73.54	.006092	164.1	53.62	.006289	159.0	39.17	.006594	151.7
	100	20	10	58.81	0.01949	51.31	42.89	0.02012	49.70	31.34	0.02110	47.39
			50	58.81	.003898	256.5	42.89	.004024	248.5	31.34	.00422	237.0
			300	58.81	.0006497	1539	42.89	.0006707	1491	31.34	.0007033	1422
	300	20	10	176.4	0.05846	17.11	128.7	0.06037	16.56	94.00	0.06330	15.8
			50	176.4	.01169	85.54	128.7	.01267	82.85	94.00	.01266	78.99
		10	100	88.2	0.001462	684.0	64.4	0.001509	662.7	47.01	0.001583	631.7
		20	100	176.4	0.005846	171.1	128.7	0.006037	165.6	94.00	0.006330	158.0
			300	176.4	.001949	513.1	128.7	.002012	497.0	94.00	.002110	473.9
	500	20	10	294.1	0.09745	10.26	214.5	0.1006	9.940	156.7	0.1055	9.479
			50	294.1	.01949	51.31	214.5	.02012	49.70	156.7	.02110	47.39
			100	294.1	.009745	102.6	214.5	.01006	99.40	156.7	.01055	94.79
		50	3	735.4	2.031	0.4924	536.2	2.096	0.4771	391.7	2.198	0.4550
			30	735.4	.2031	4.924	536.2	.2096	4.771	391.7	.2198	4.550
			100	735.4	.06092	16.41	536.2	.06289	15.90	391.7	.06594	15.17
Drizzle	100	400	10	1176	7.796	0.1283	857.7	8.050	0.1242	626.7	8.442	0.1185
	300	400	100	3529	2.339	0.4275	2574	2.415	0.4141	1880	2.532	0.3949
			300	3529	.7797	1.283	2574	.8050	1.242	1880	.8440	1.185
	500	400	300	5882	1.299	0.7698	4289	1.342	0.7452	3134	1.407	0.7107
Rain	300	1000	50	8823	29.24	0.03420	6434	30.18	0.03313	4701	31.66	0.03159
			100	8823	14.62	.06840	6434	15.09	.06627	4701	15.83	.06317
			300	8823	4.873	.20520	6434	5.030	.1988	4701	5.277	.1895

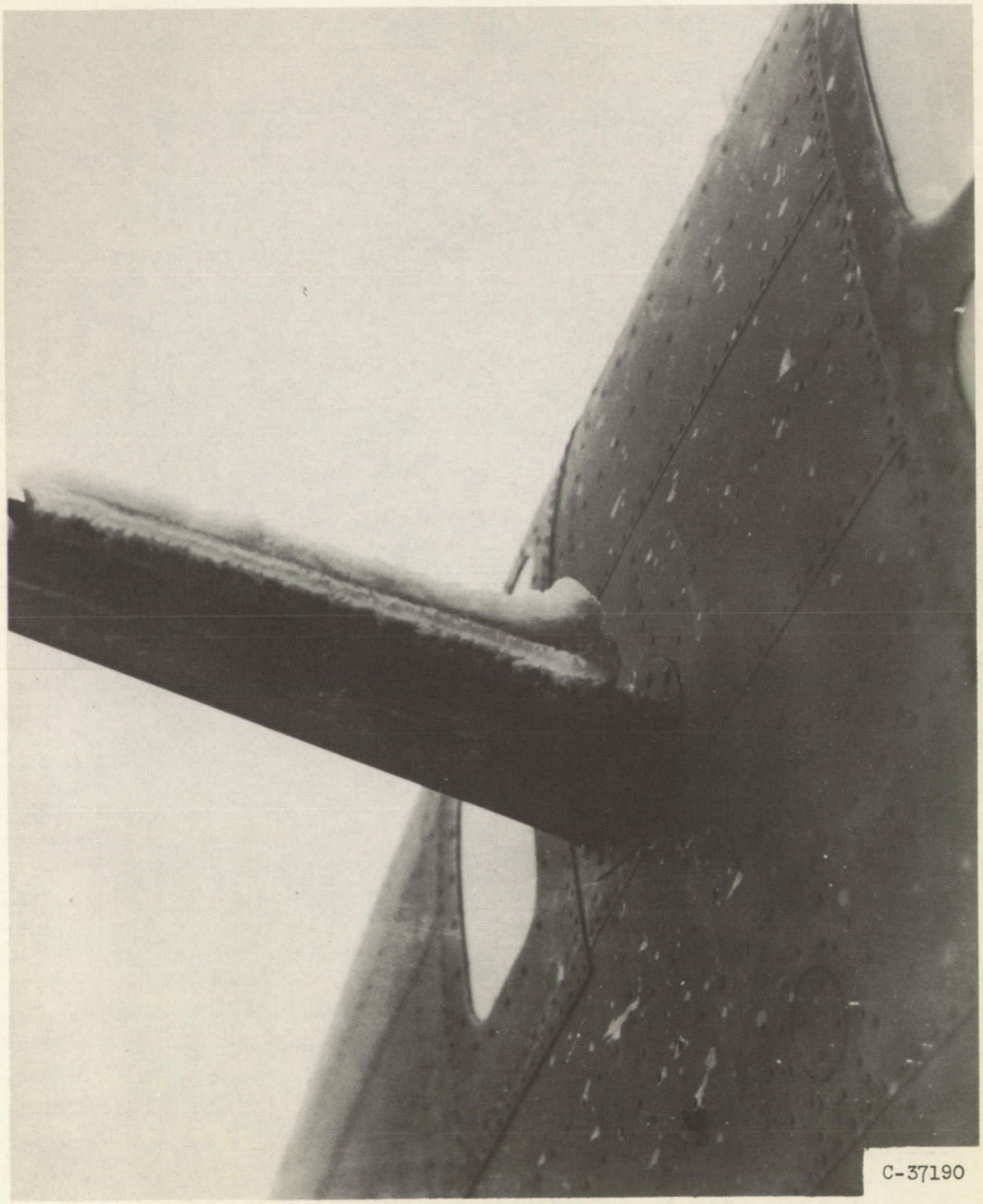

Figure 1. - Ice formation on pitot mast on B-24 aircraft after flight through supercooled clouds.

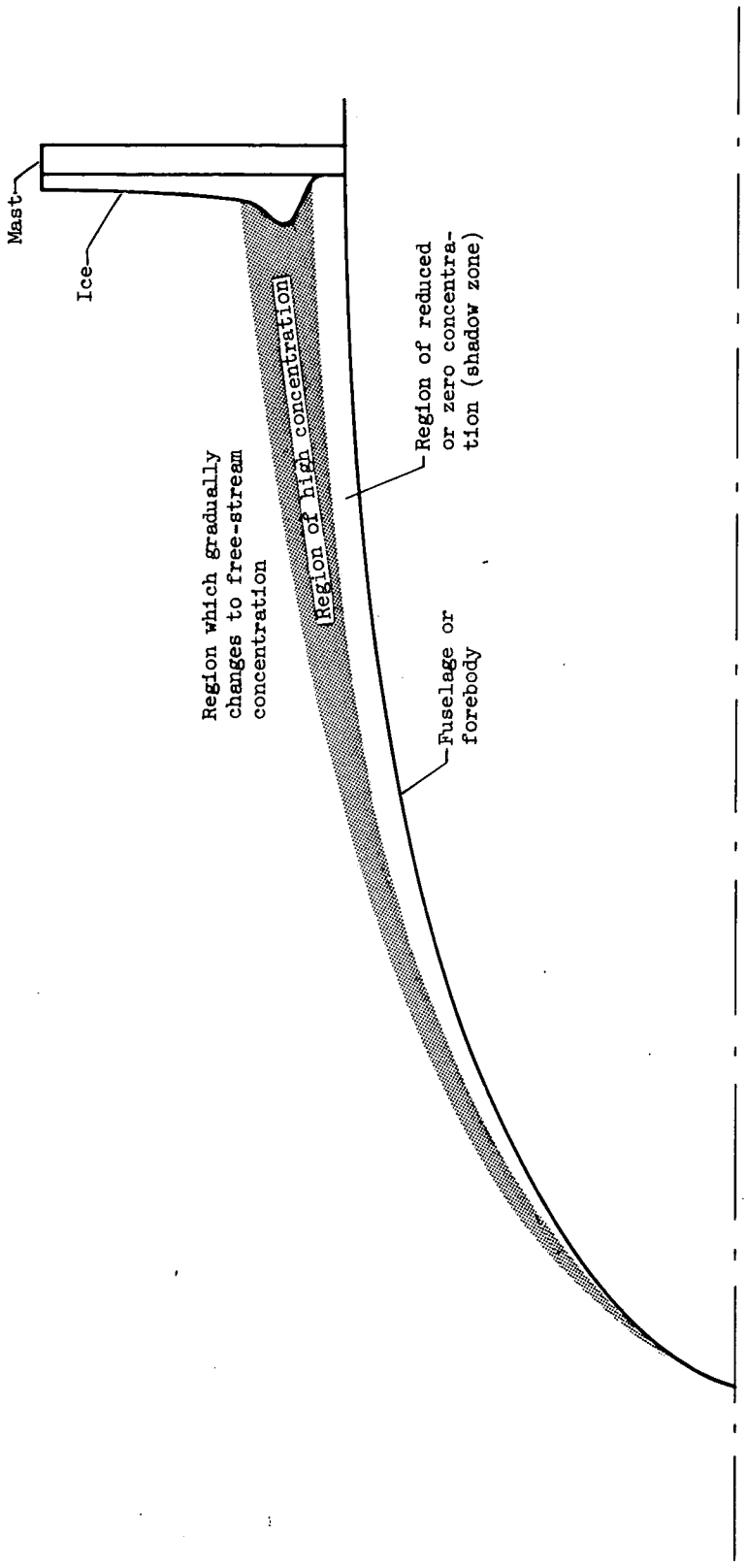

Figure 2. - Sketch of regions of varying droplet concentration around fore part of fuselage.

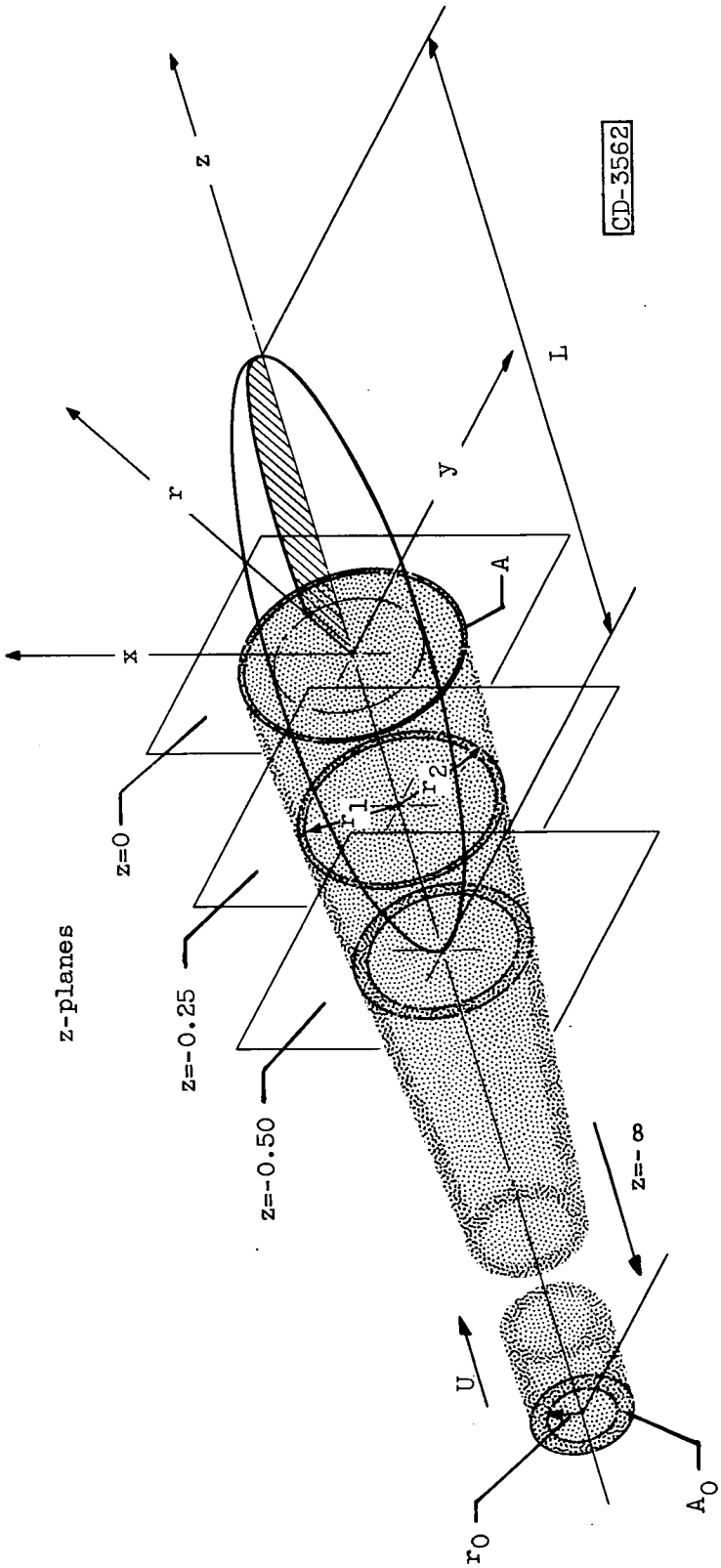

Figure 3. - Coordinate system for droplet trajectory calculations.

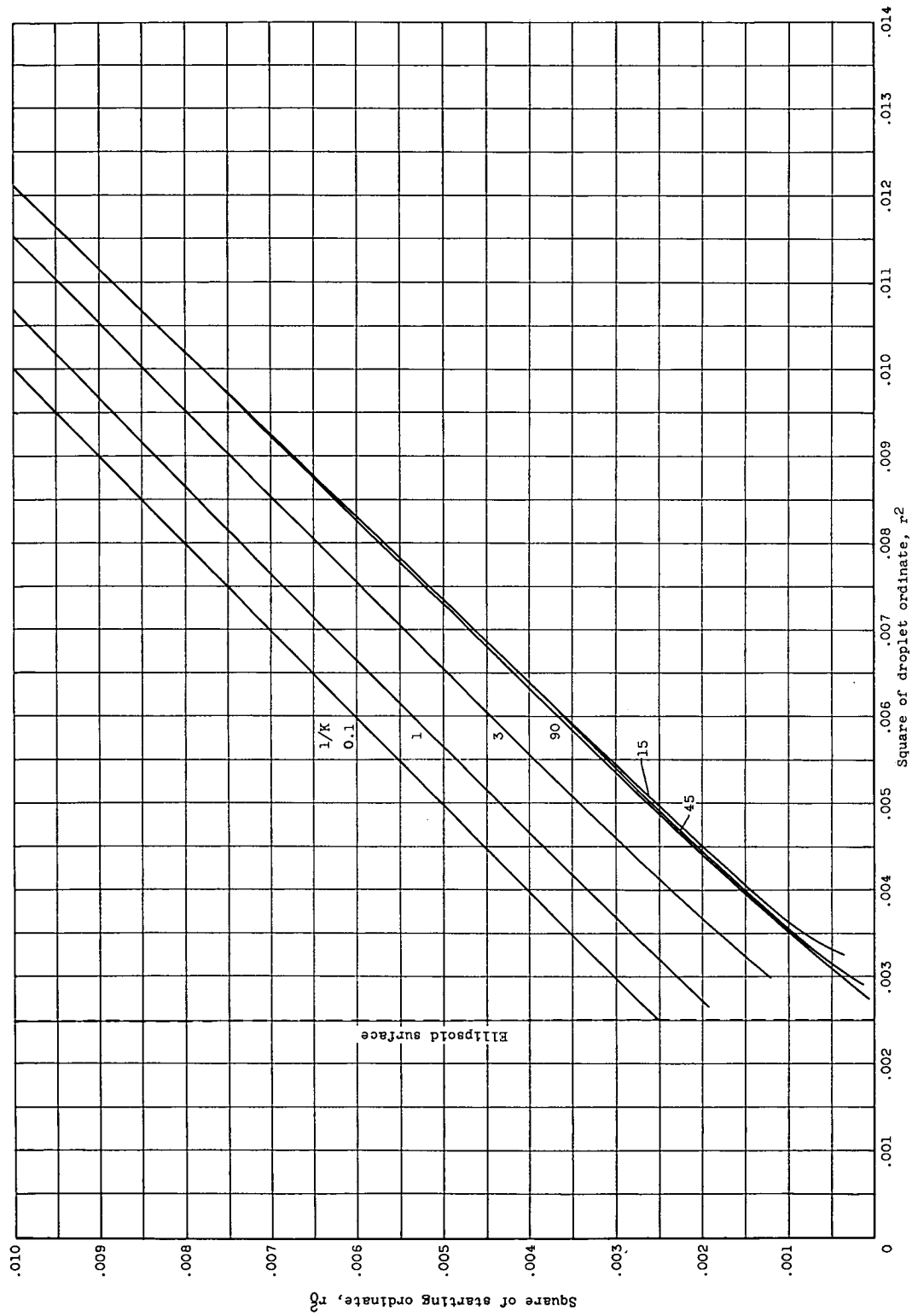

(a) $z = 0$; $Re_0 = 0$.

Figure 4. - Square of starting ordinate as function of square of droplet ordinate at constant z-position.

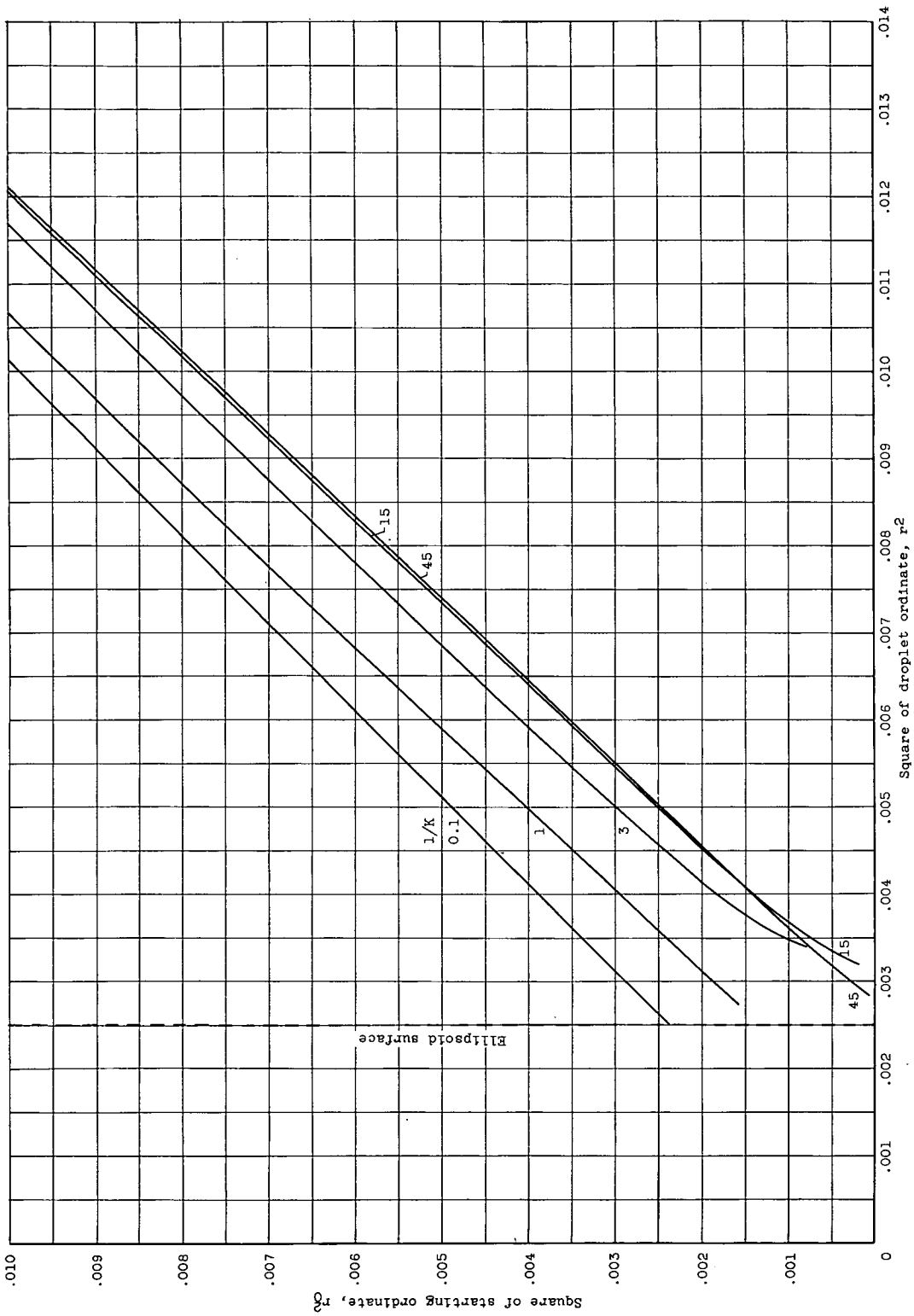

(b) $z = 0$; $Re_0 = 128$.

Figure 4. - Continued. Square of starting ordinate as function of square of droplet ordinate at constant z-position.

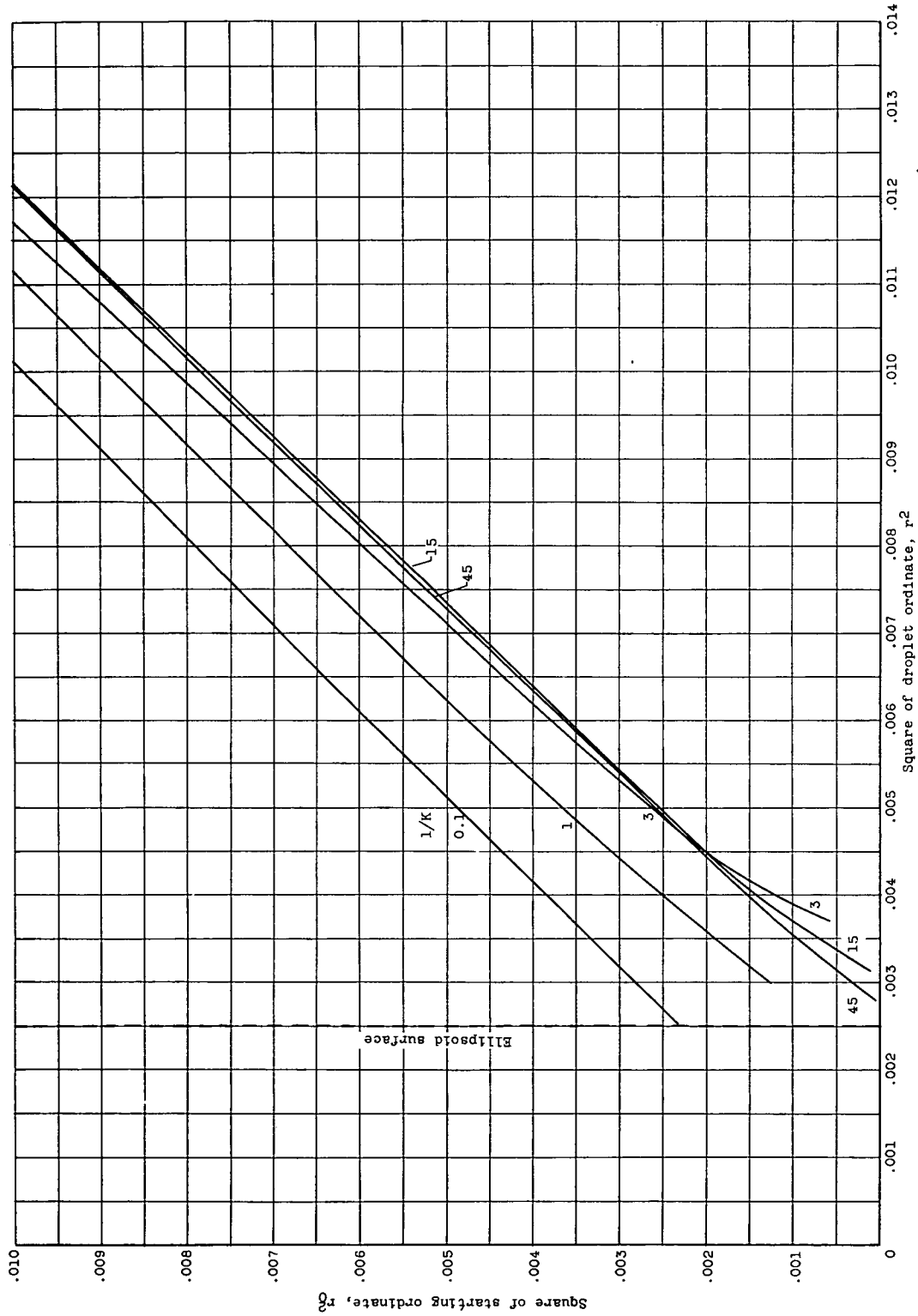

Figure 4. - Continued. Square of starting ordinate as function of square of droplet ordinate at constant z-position.

(c) $z = 0$; $Re_0 = 512$.

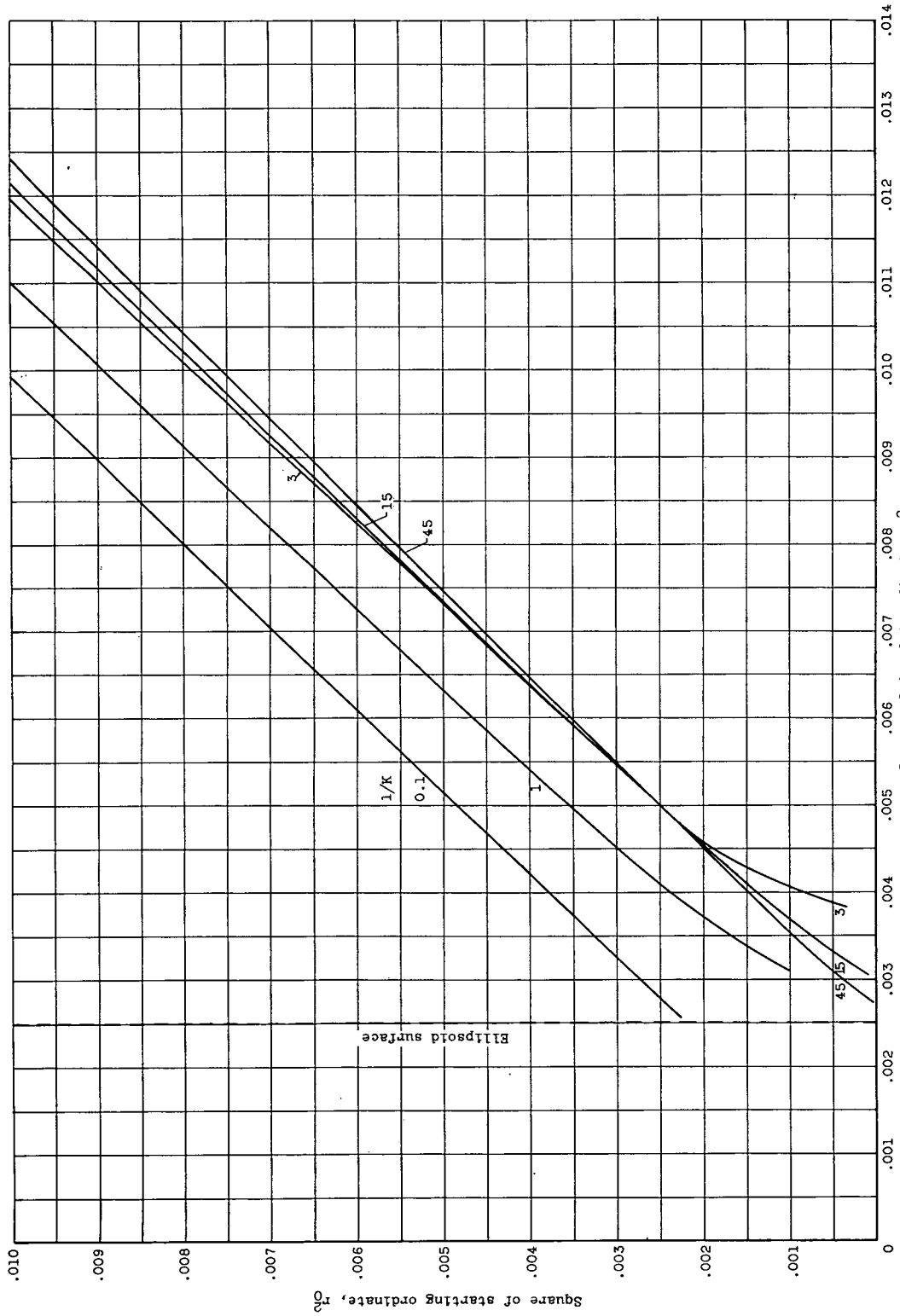

(d) $z = 0$; $Re_0 = 1024$.

Figure 4. - Continued. Square of starting ordinate as function of square of droplet ordinate at constant z-position.

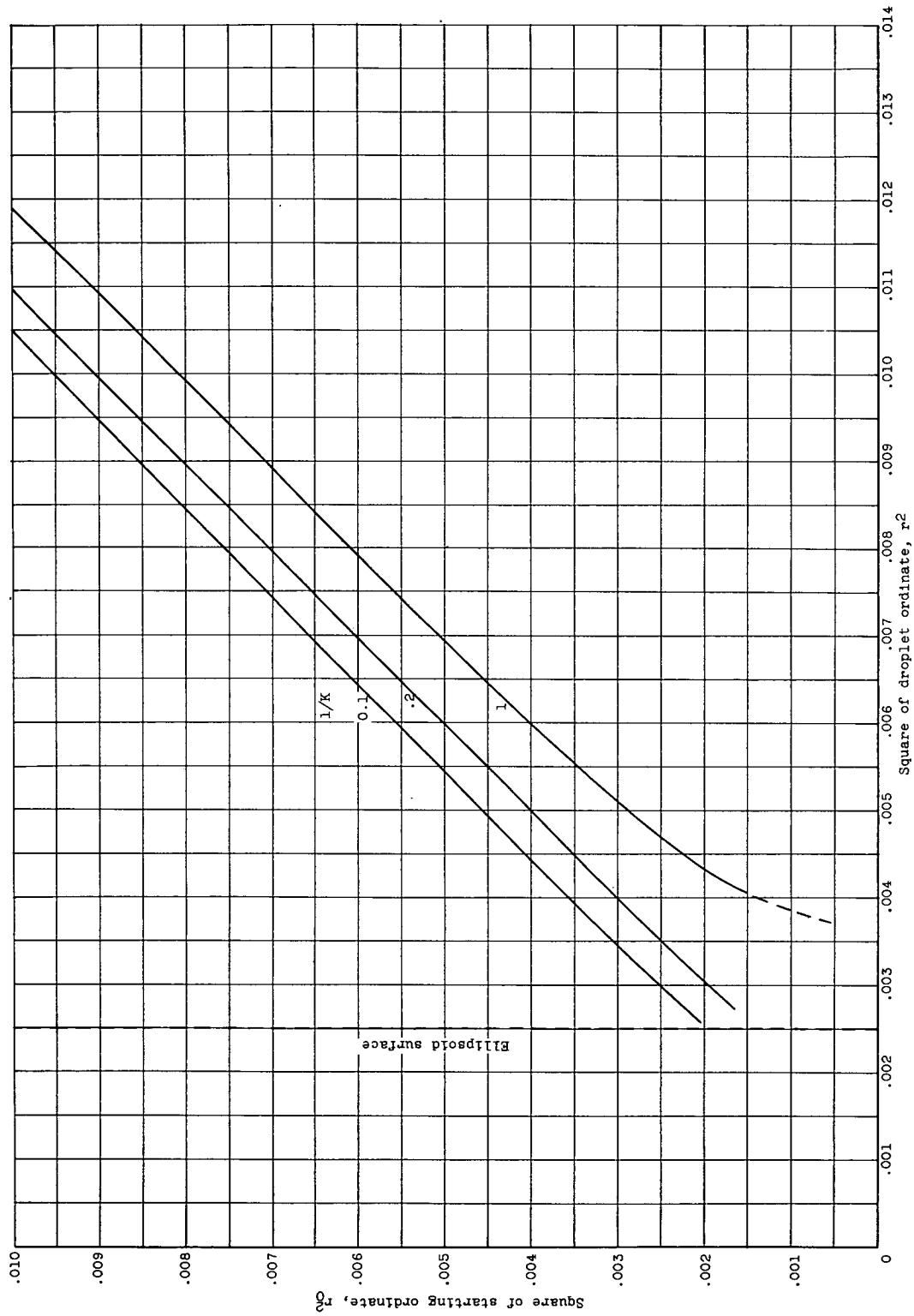

(e) $z = 0$; $Re_0 = 4096$.

Figure 4. - Continued. Square of starting ordinate as function of square of droplet ordinate at constant z-position.

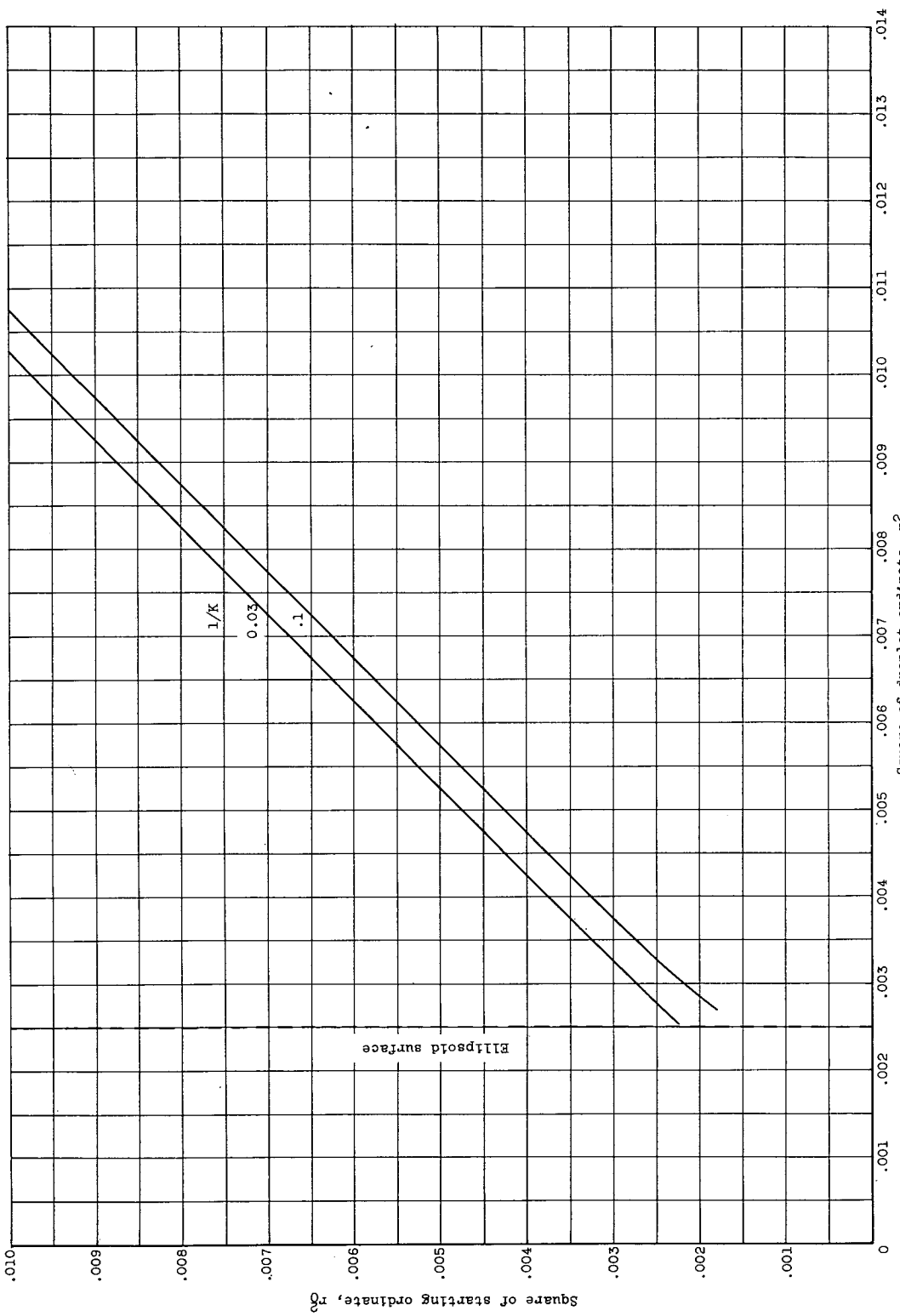

Figure 4. - Continued. Square of starting ordinate as function of square of droplet ordinate at constant z-position.

(f) $z = 0$; $Re_0 = 8192$.

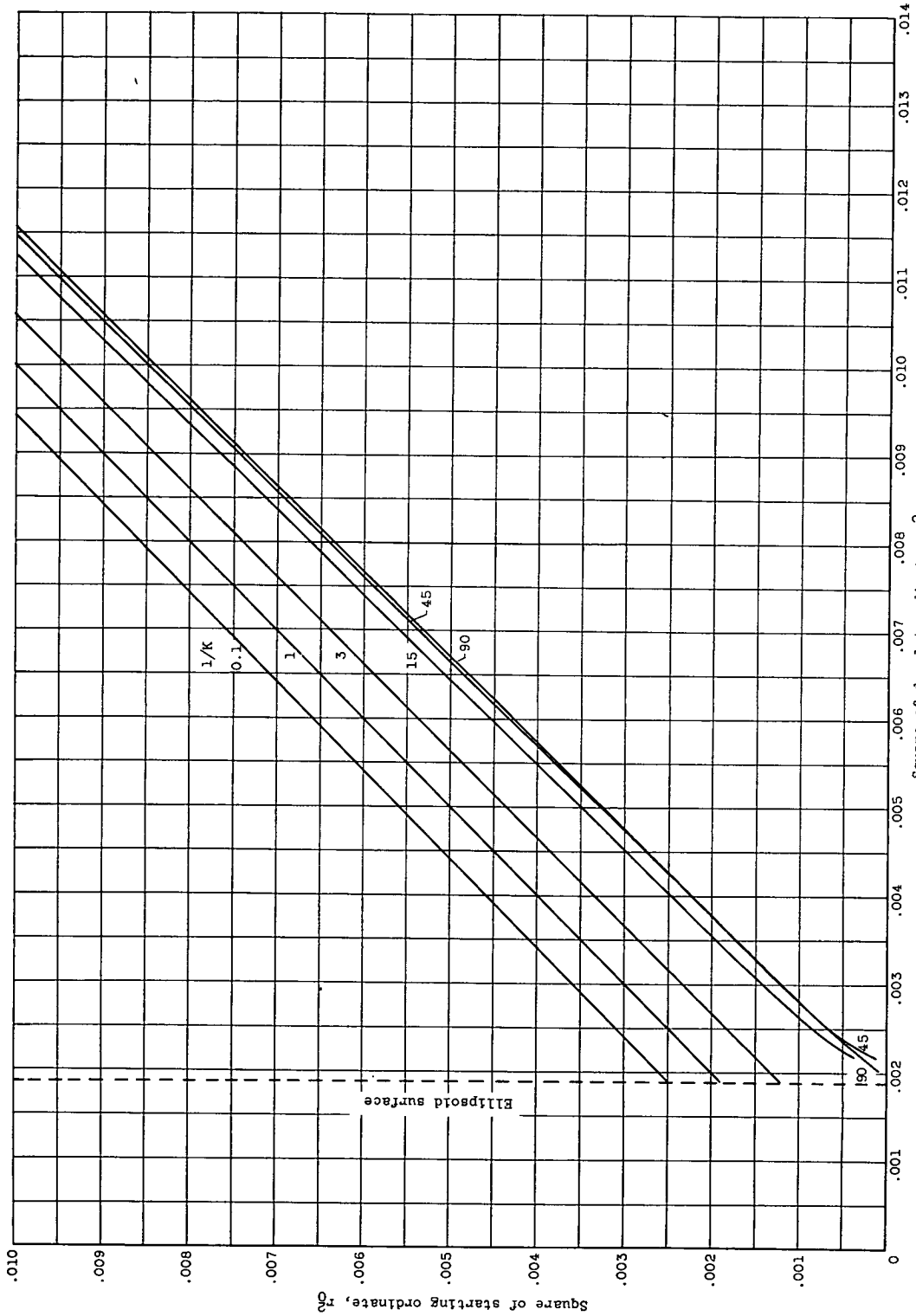

(g) $z = -0.25$; $Re_0 = 0$.

Figure 4. - Continued. Square of starting ordinate as function of square of droplet ordinate at constant z-position.

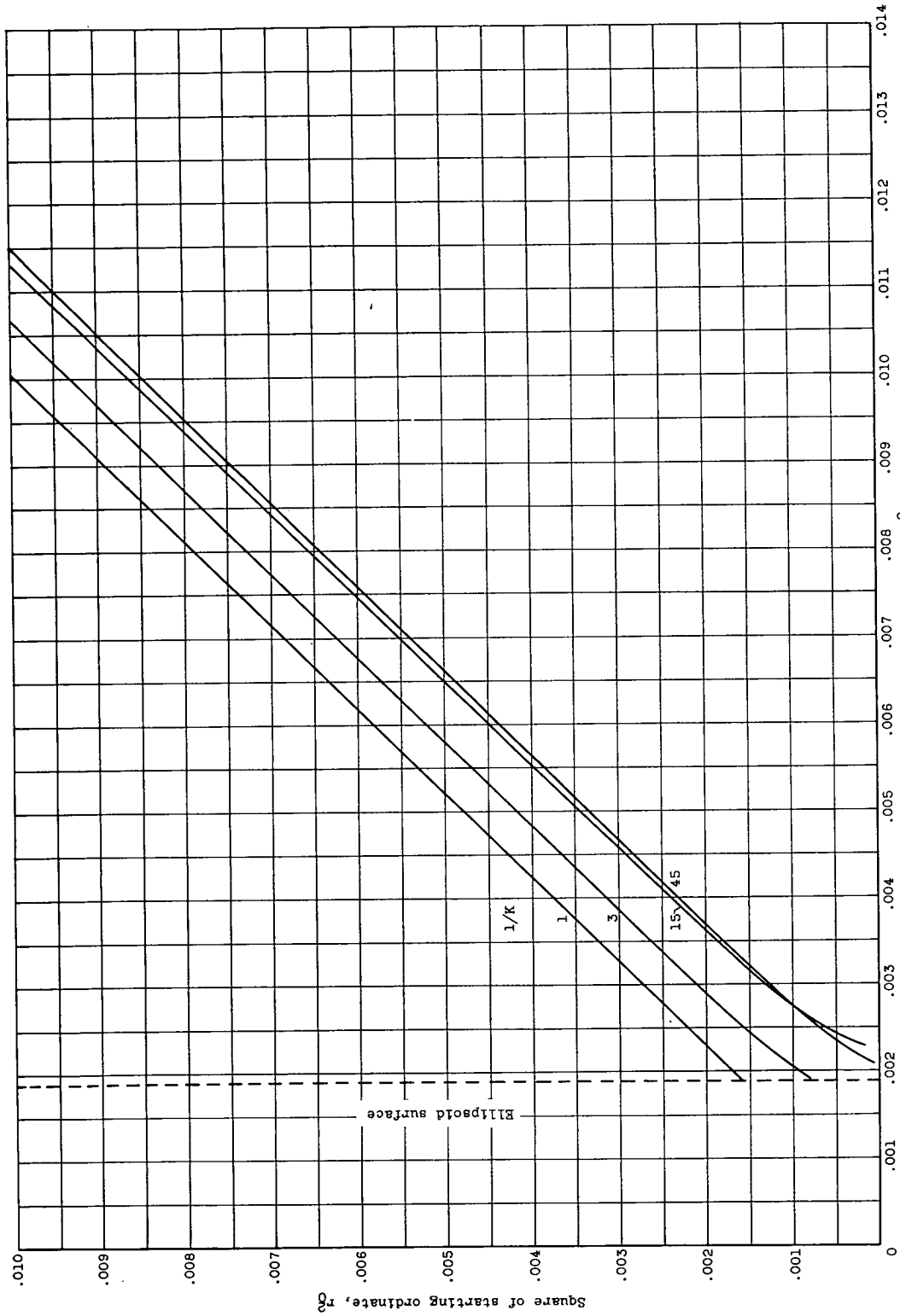

(h) z = -0.25; Re_0 = 128.

Figure 4. - Continued. Square of starting ordinate as function of square of droplet ordinate at constant z-position.

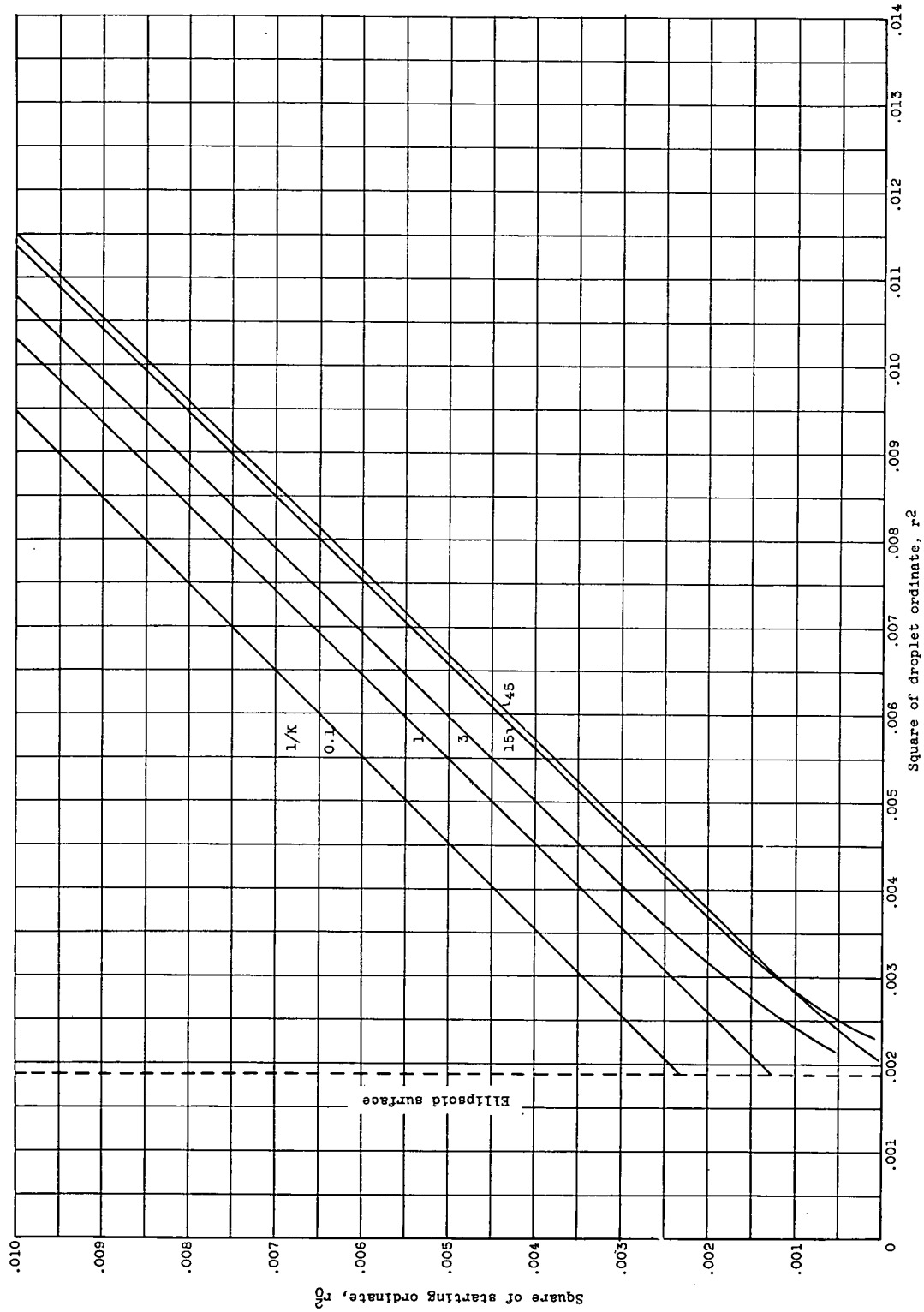

(1) $z = -0.25$; $Re_0 = 512$.

Figure 4. - Continued. Square of starting ordinate as function of square of droplet ordinate at constant z-position.

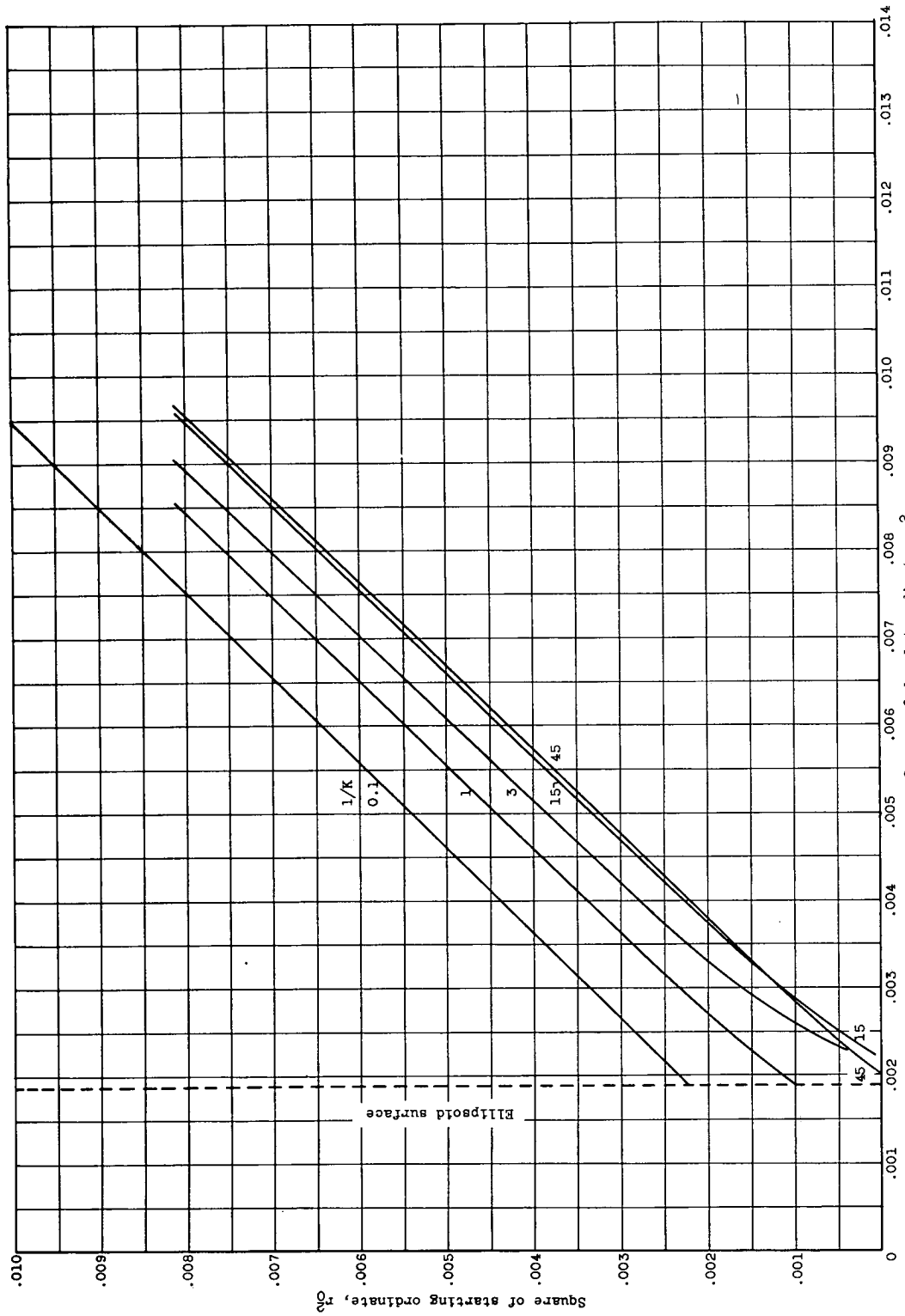

(j) $z = -0.25$; $Re_0 = 1024$.

Figure 4. - Continued. Square of starting ordinate as function of square of droplet ordinate at constant z-position.

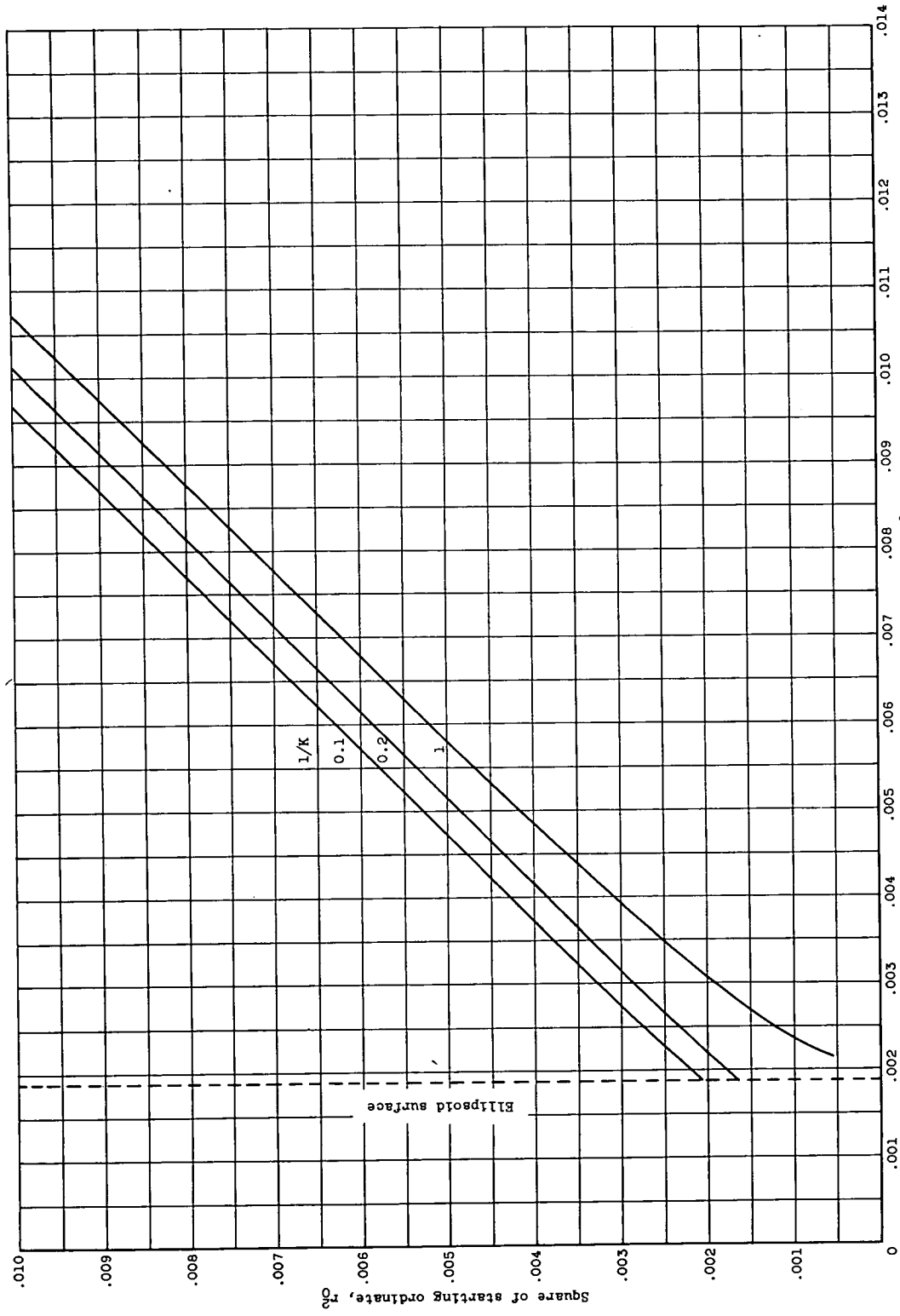

(k) $z = -0.25$; $Re_0 = 4096$.

Figure 4. - Continued. Square of starting ordinate as function of square of droplet ordinate at constant z-position.

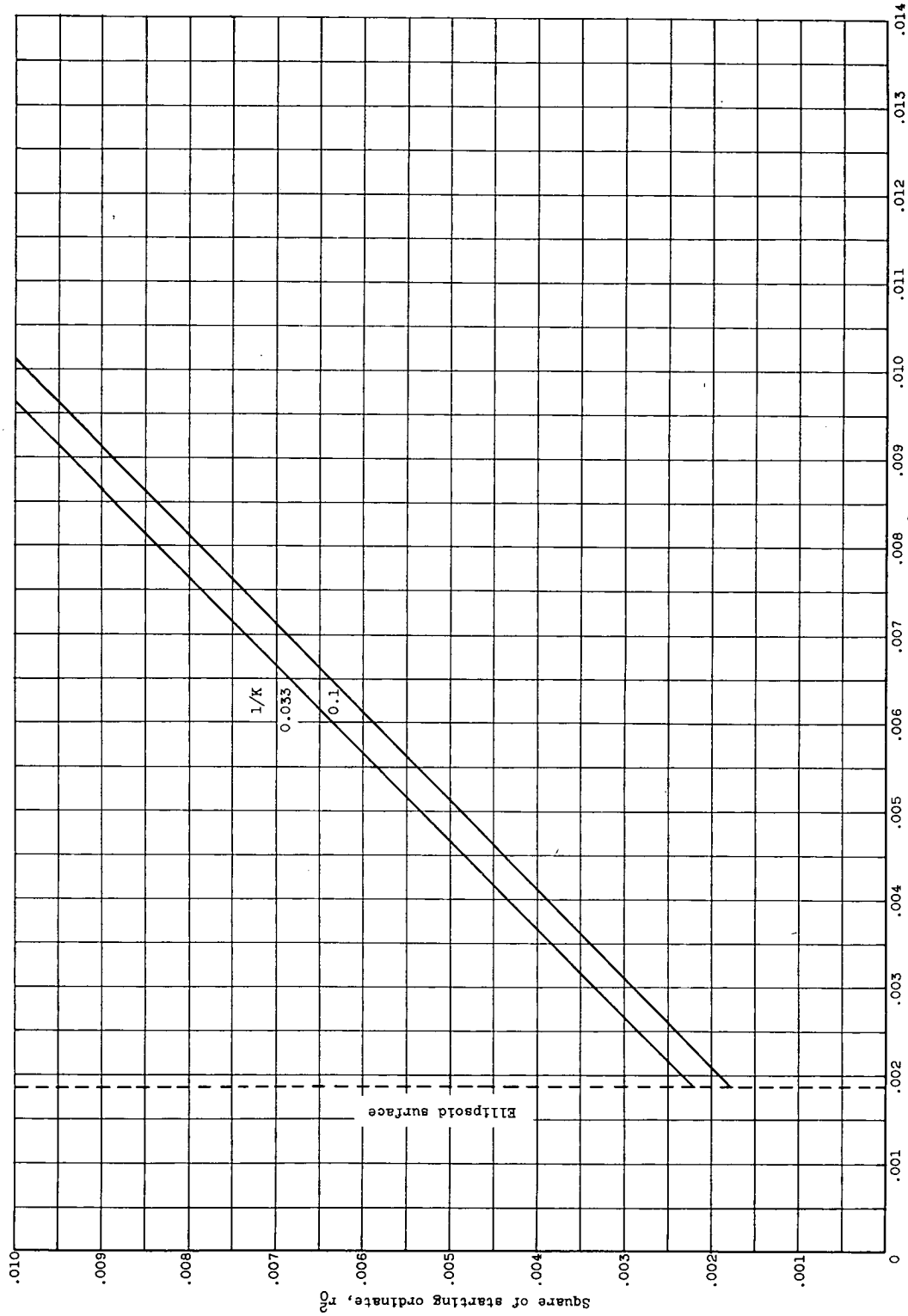

(*l*) $z = -0.25$; $Re_0 = 8192$.

Figure 4. - Continued. Square of starting ordinate as function of square of droplet ordinate at constant z-position.

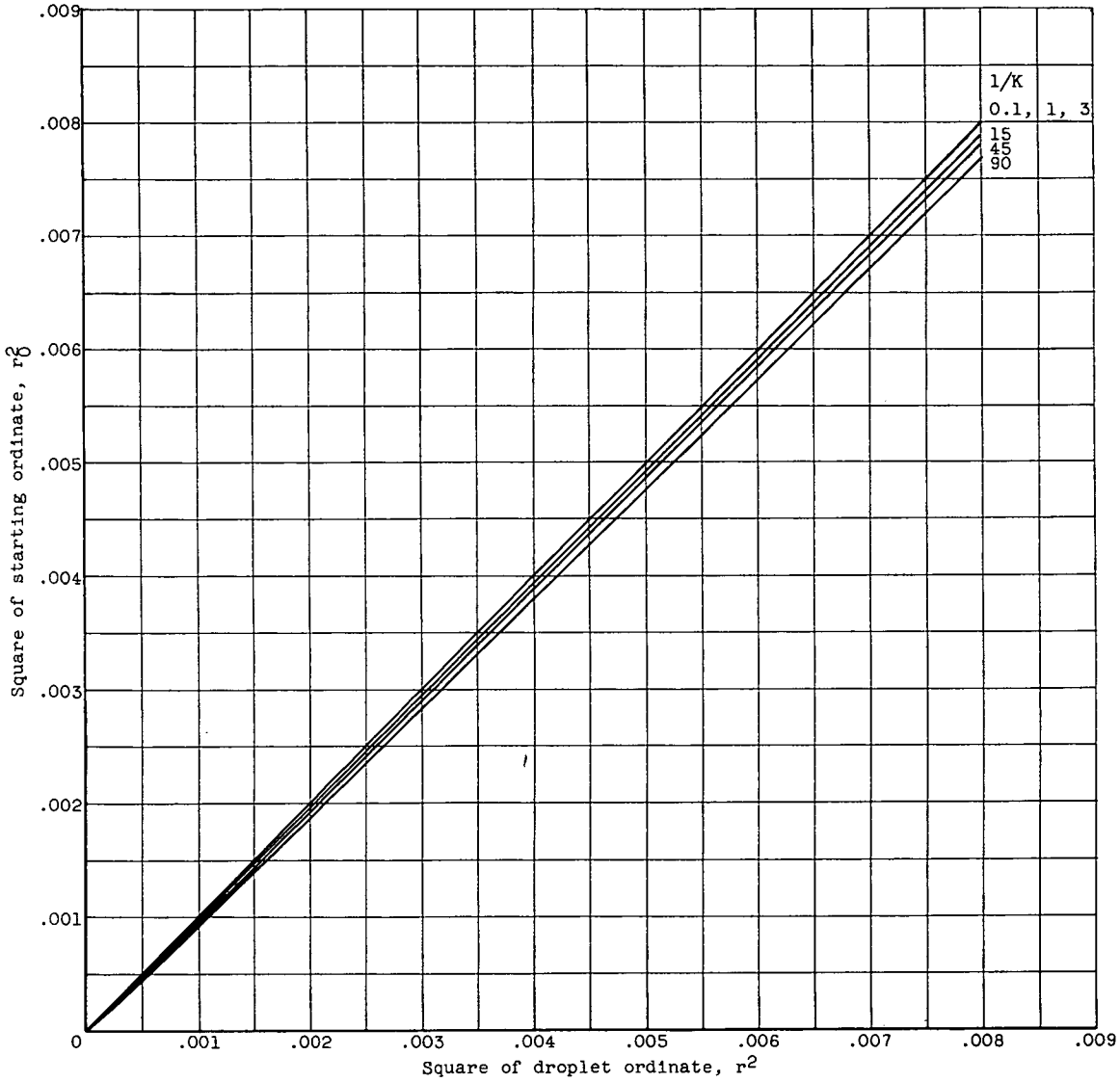

(m) z = -0.5; Re_0 = 0, 128, 512, 1024, 4096, and 8192.

Figure 4. - Concluded. Square of starting ordinate as function of square of droplet ordinate at constant z-position.

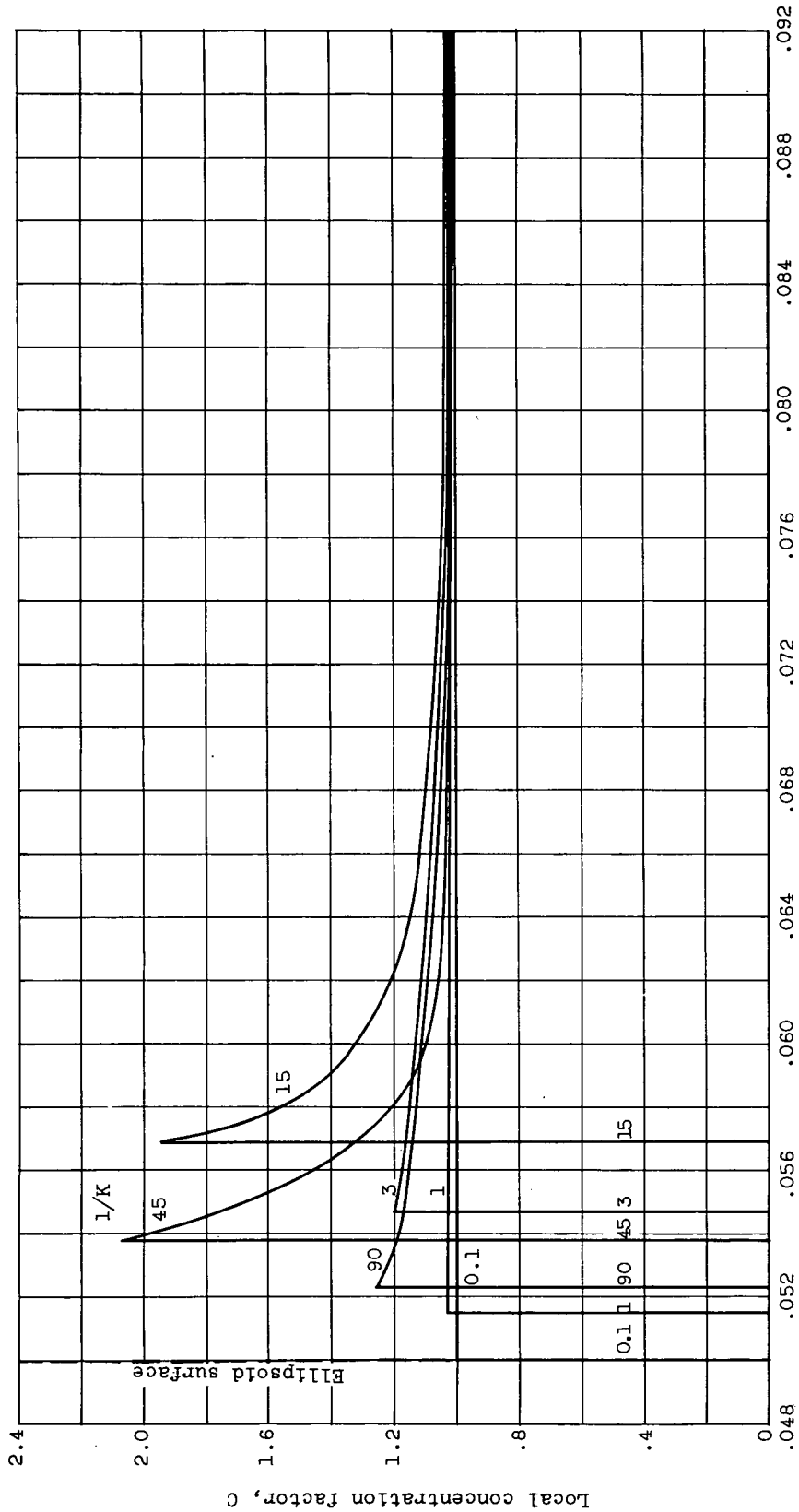

(a) $z = 0$; $Re_0 = 0$.

Figure 5. - Variation of local concentration factor with radial distance r at constant axial position z.

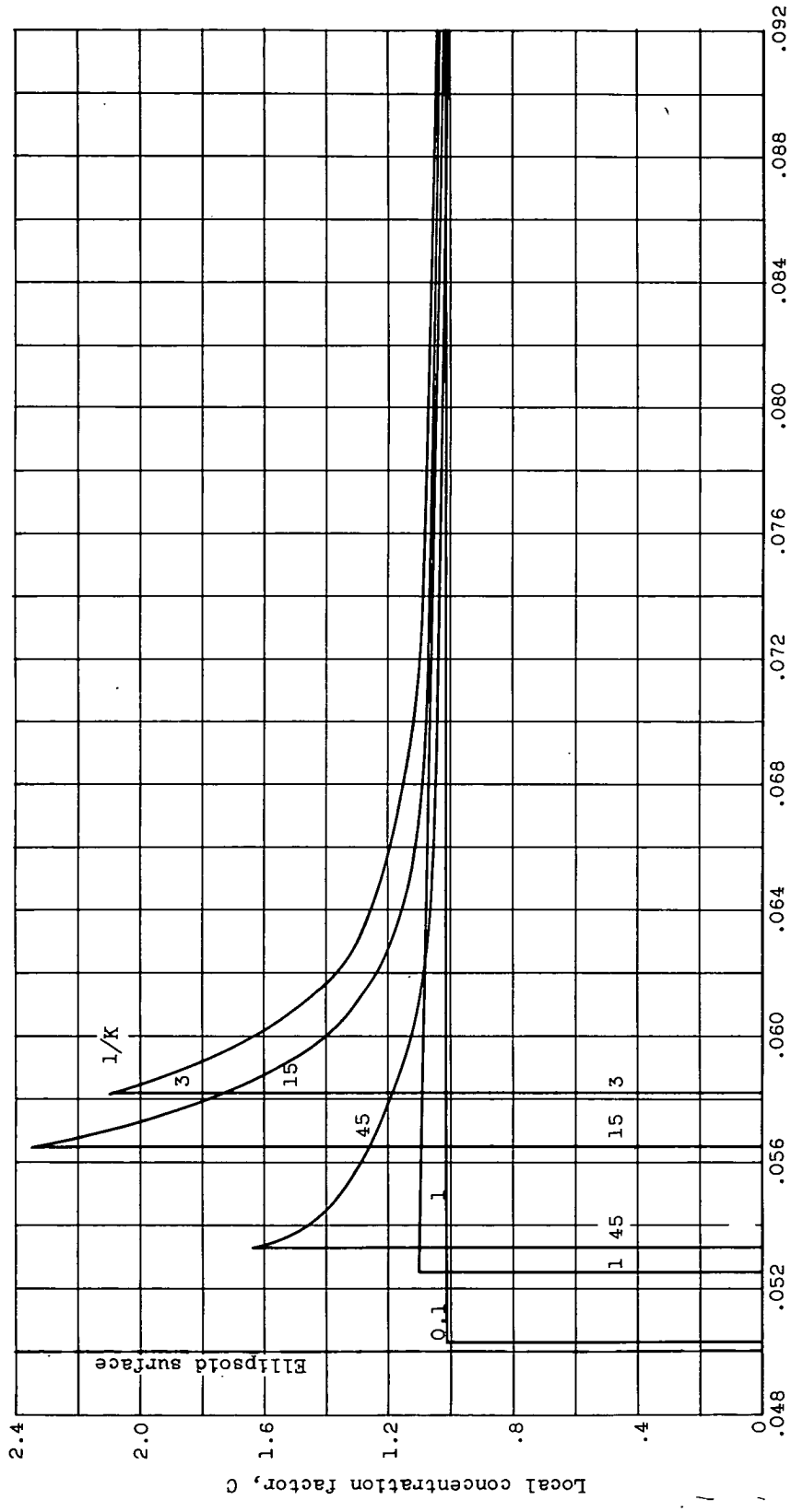

(b) z = 0; Re_0 = 128.

Figure 5. - Continued. Variation of local concentration factor with radial distance r at constant axial position z.

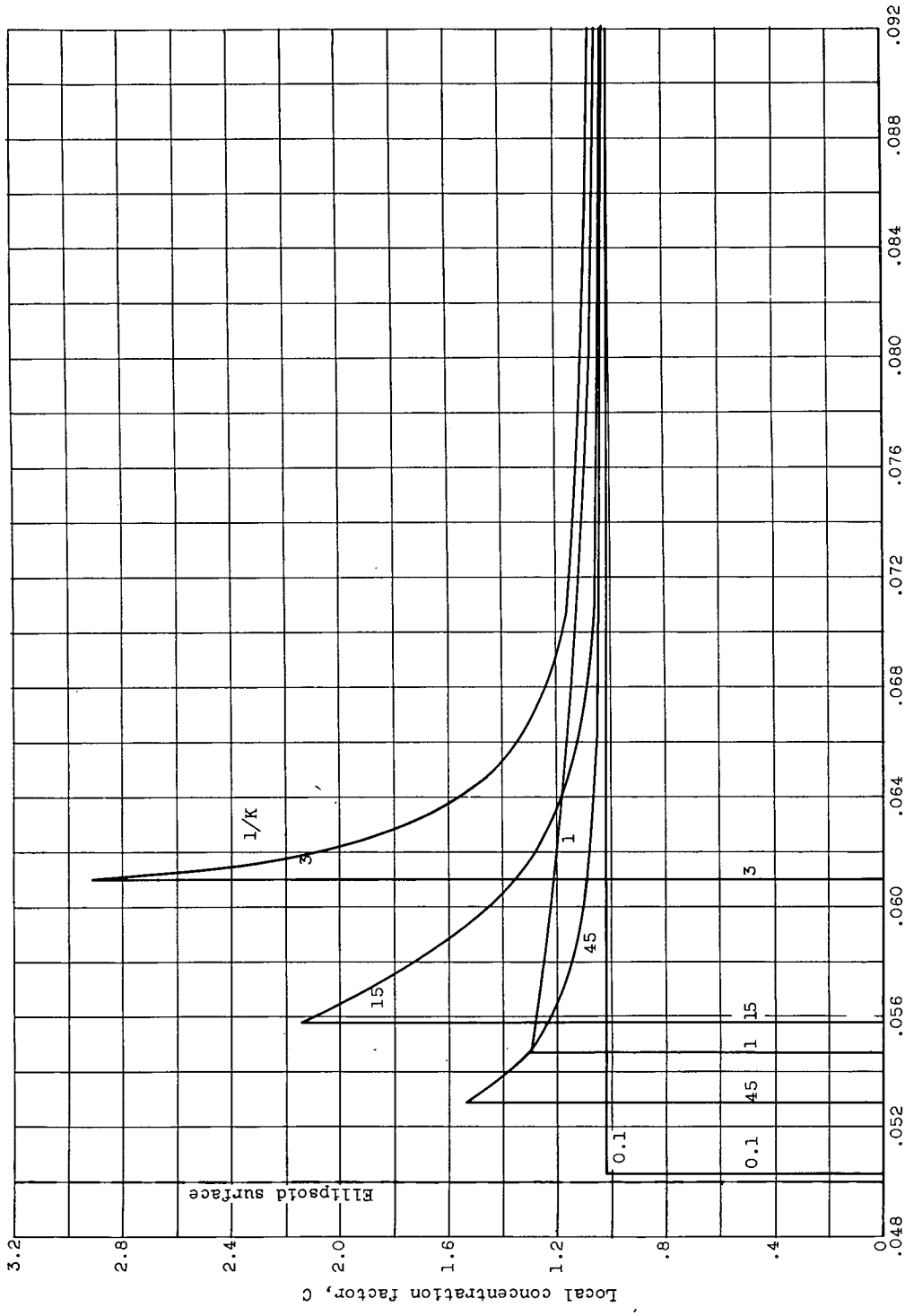

(c) $z = 0$; $Re_0 = 512$.

Figure 5. - Continued. Variation of local concentration factor with radial distance r at constant axial position z.

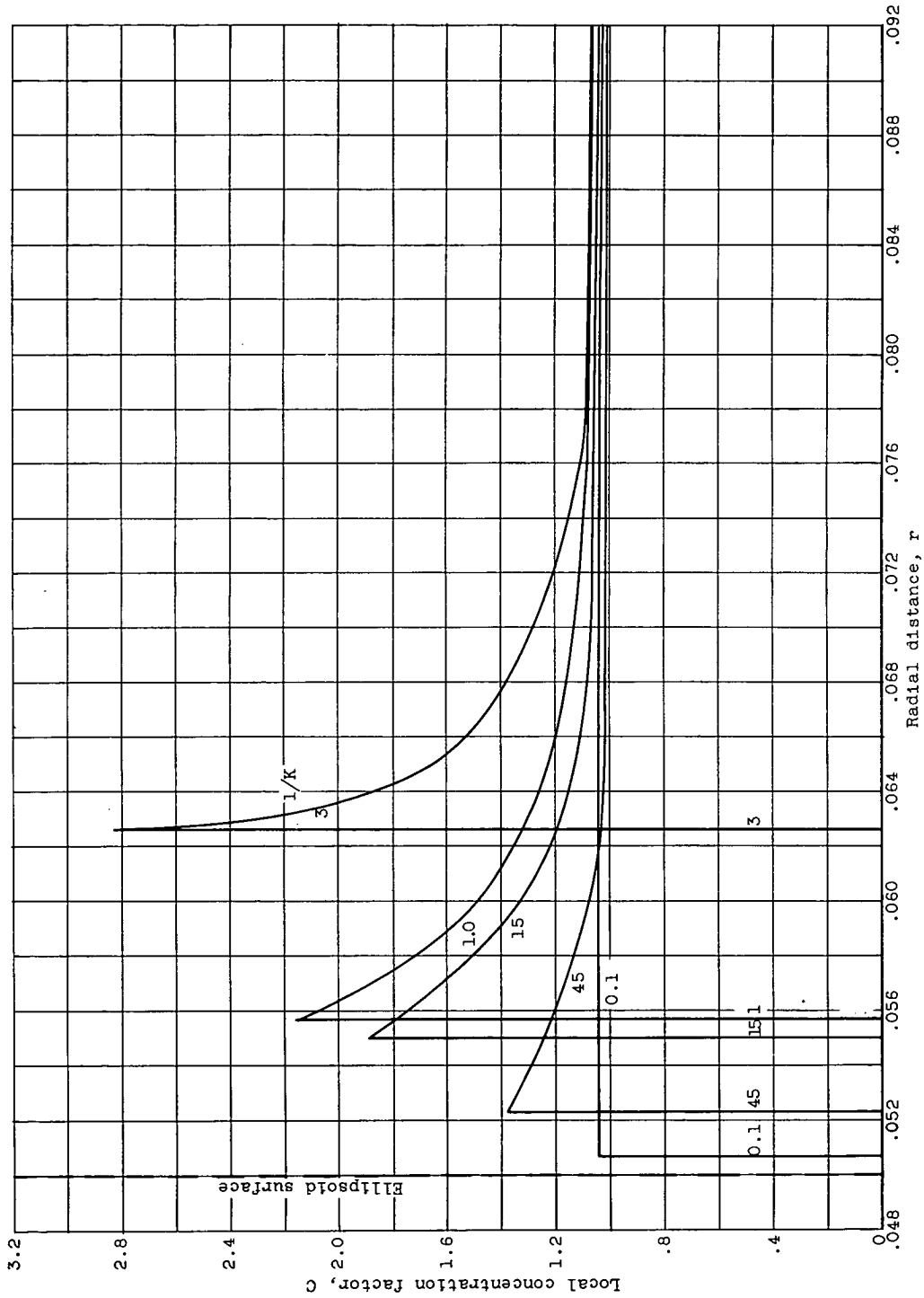

(d) $z = 0$; $Re_0 = 1024$.

Figure 5. - Continued. Variation of local concentration factor with radial distance r at constant axial position z.

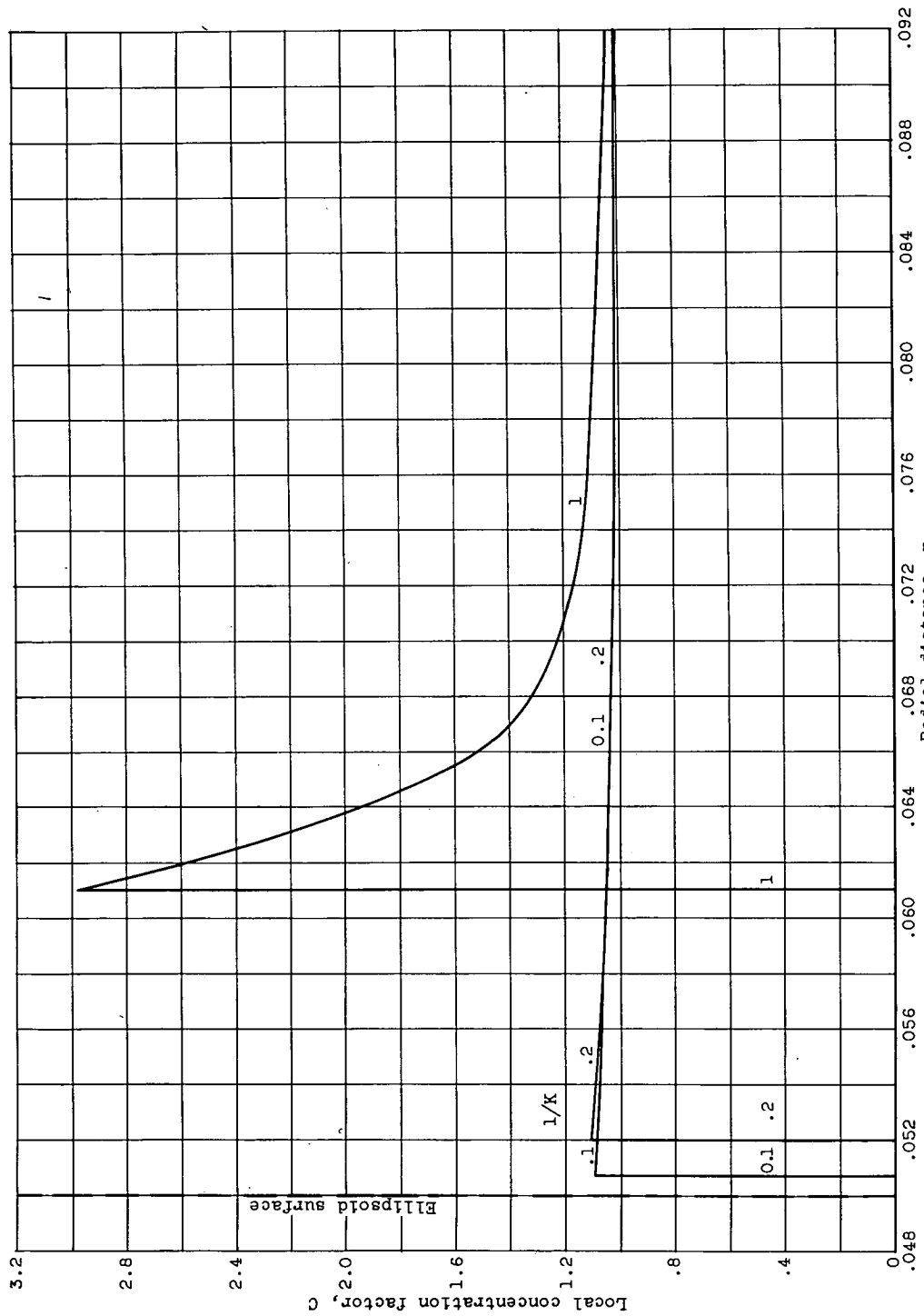

(e) $z = 0$; $Re_0 = 4096$.

Figure 5. - Continued. Variation of local concentration factor with radial distance r at constant axial position z.

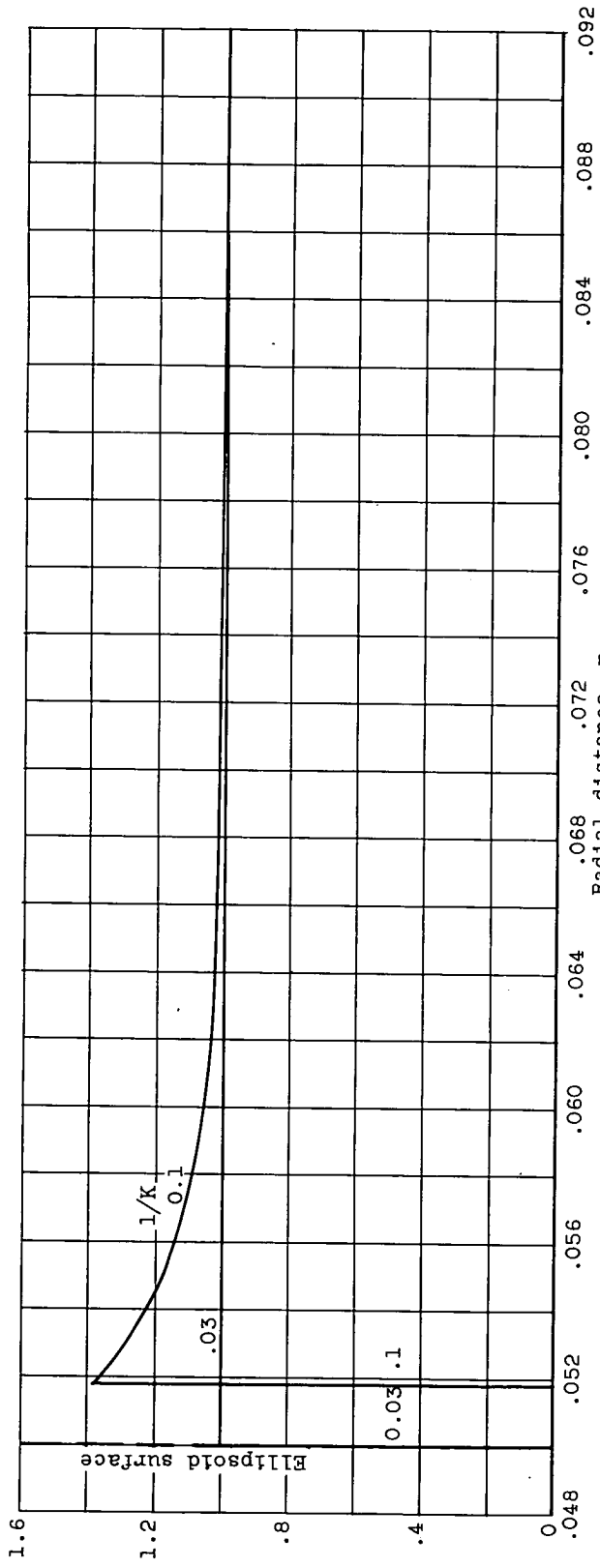

(f) $z = 0$; $Re_0 = 8192$.

Figure 5. - Continued. Variation of local concentration factor with radial distance r at constant axial position z.

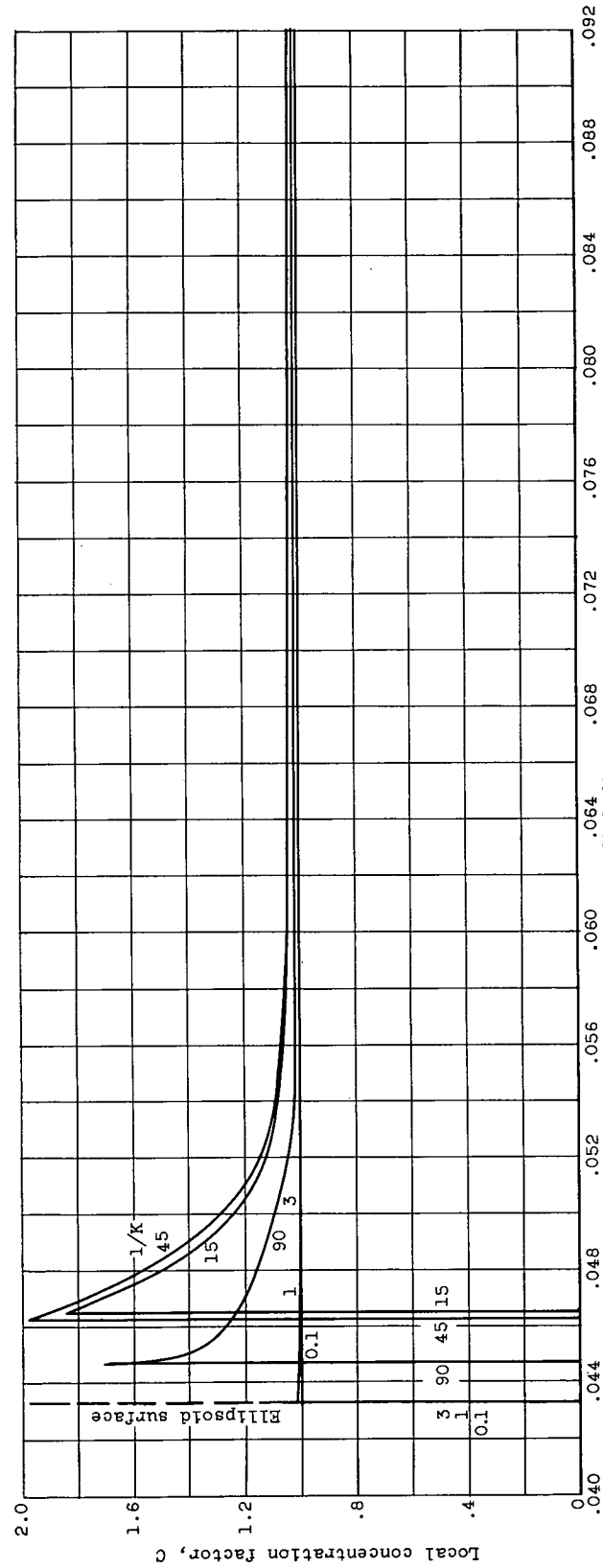

(g) $z = -0.25$; $Re_O = 0$.

Figure 5. - Continued. Variation of local concentration factor with radial distance r at constant axial position z.

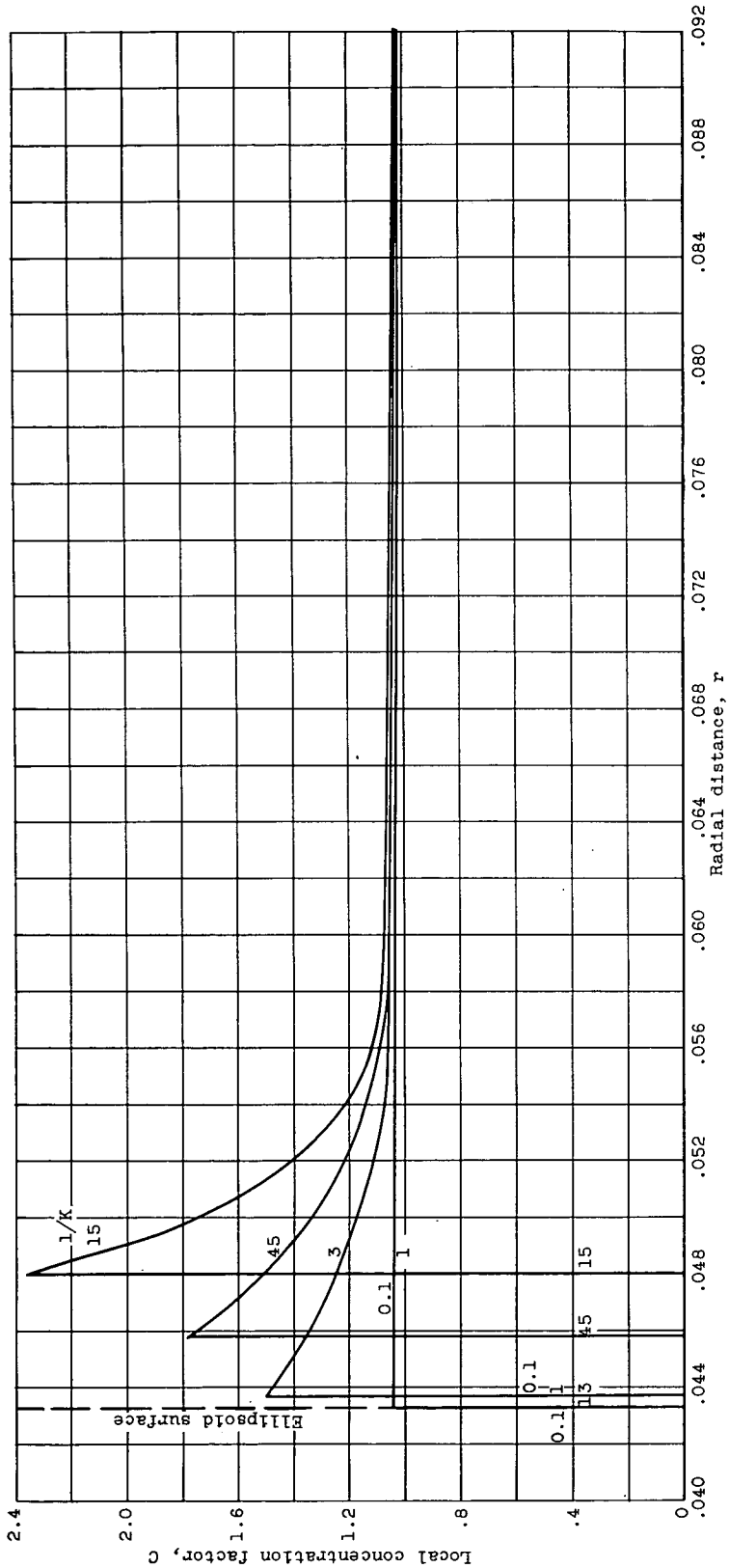

(h) $z = -0.25$; $Re_0 = 128$.

Figure 5. - Continued. Variation of local concentration factor with radial distance r at constant axial position z.

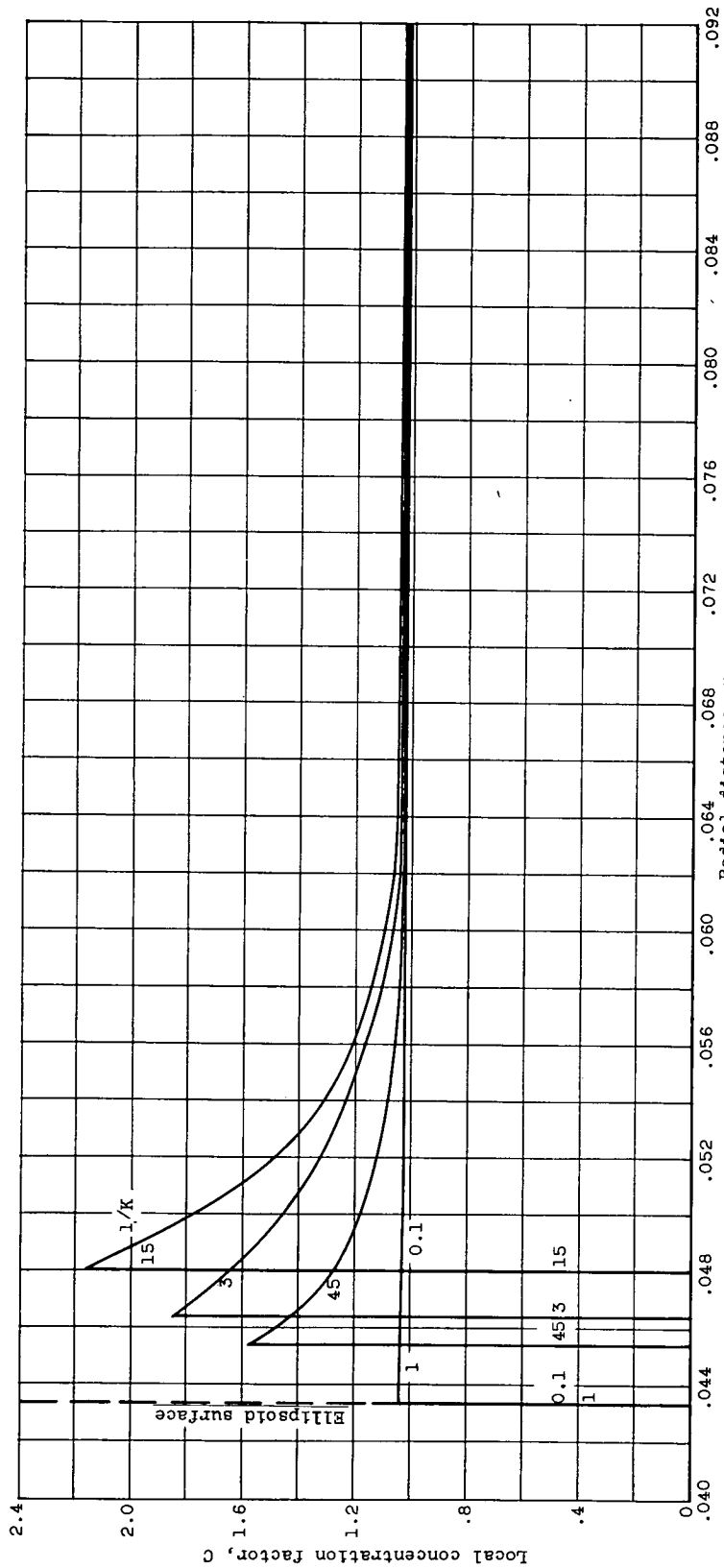

(1) $z = -0.25$; $Re_0 = 512$.

Figure 5. - Continued. Variation of local concentration factor with radial distance r at constant axial position z.

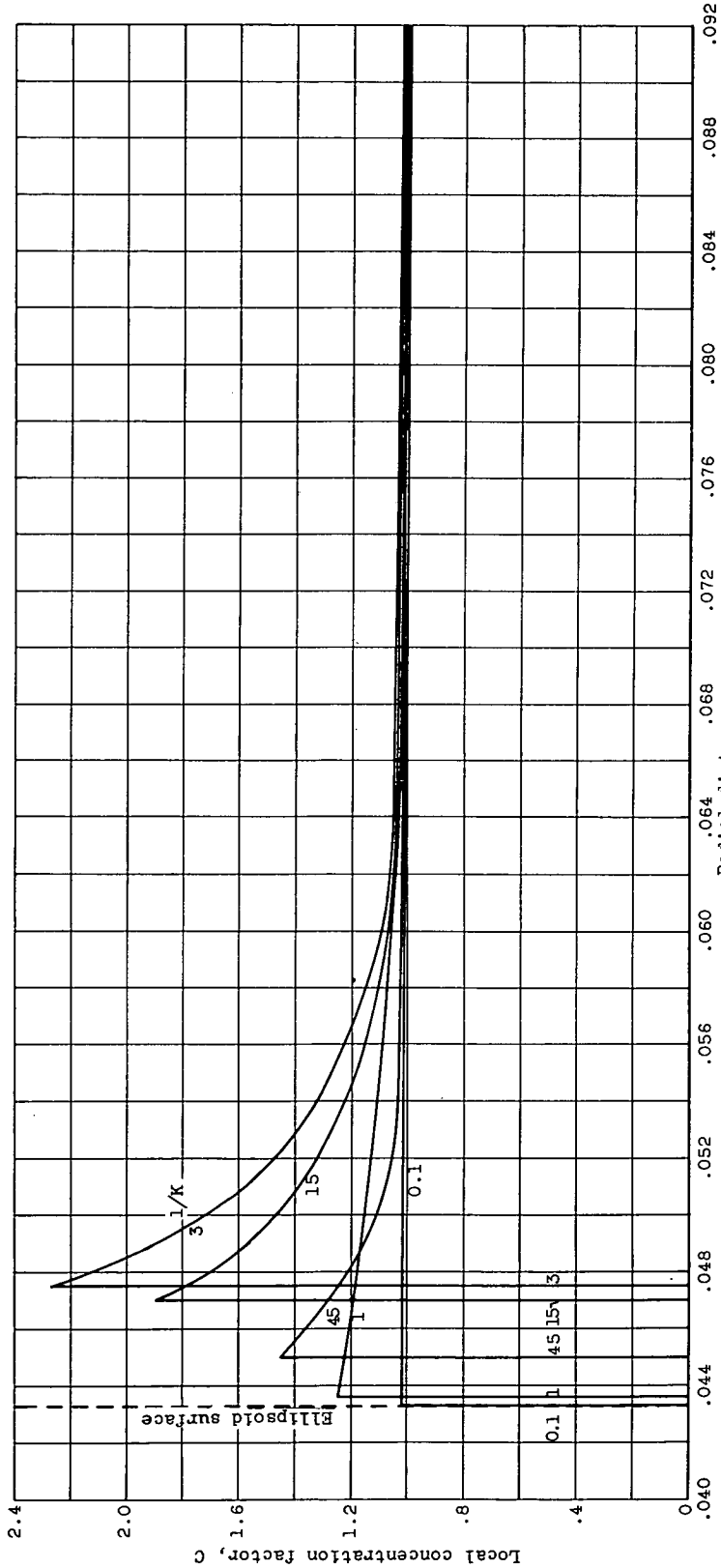

(j) $z = -0.25$; $Re_0 = 1024$.

Figure 5. - Continued. Variation of local concentration factor with radial distance r at constant axial position z.

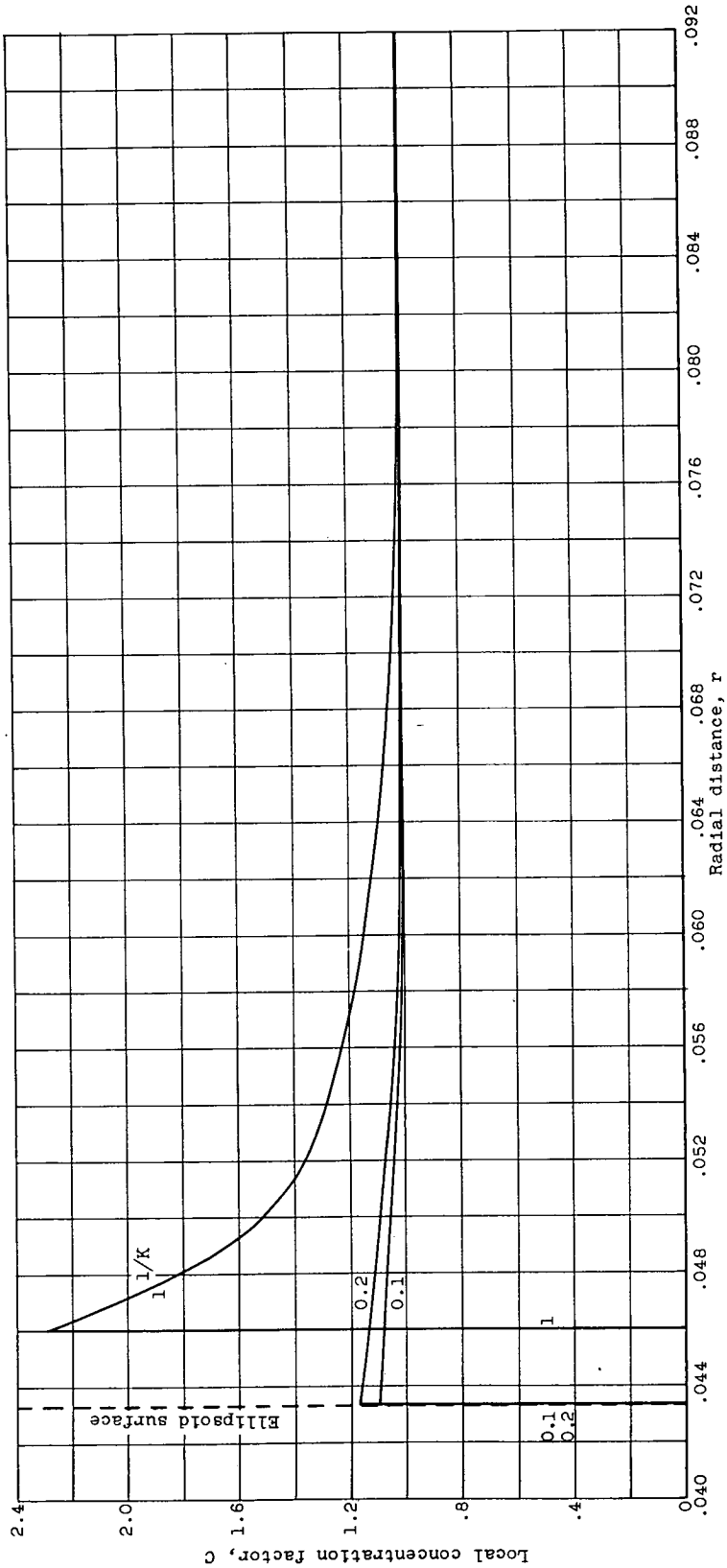

(k) $z = -0.25$; $Re_0 = 4096$.

Figure 5. - Continued. Variation of local concentration factor with radial distance r at constant axial position z.

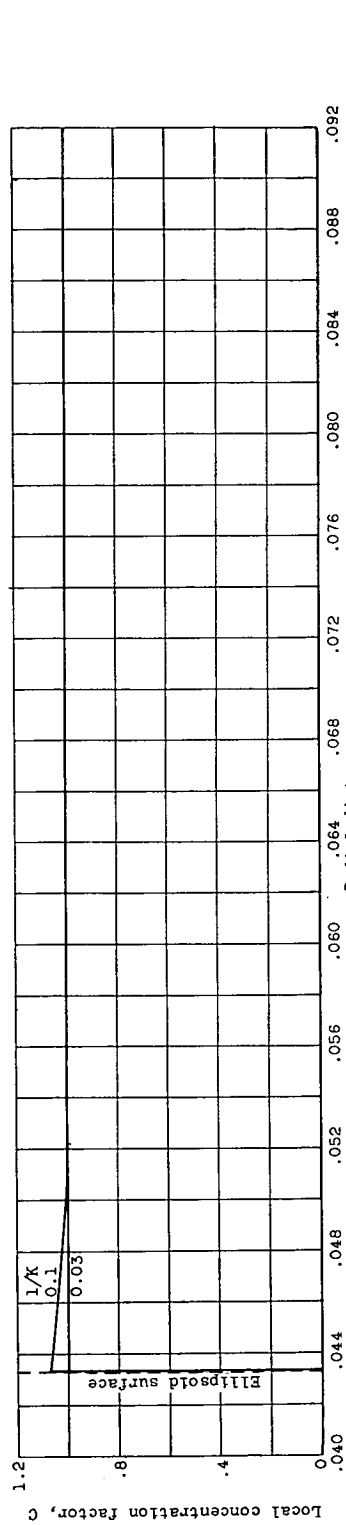

(l) $z = -0.25$; $Re_0 = 8192$.

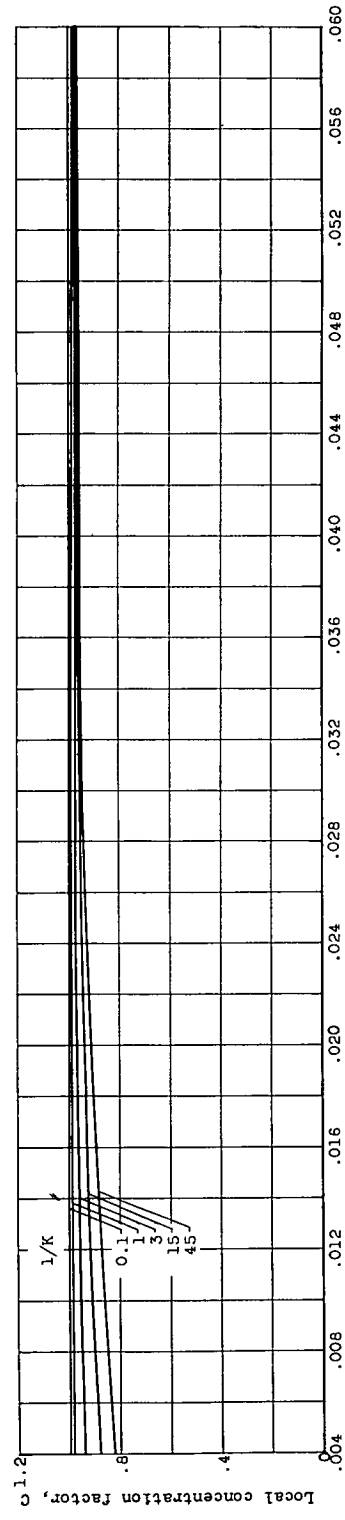

(m) $z = -0.5$; $Re_0 = 0$, 128, 512, 1024, 4096, and 8192.

Figure 5. - Concluded. Variation of local concentration factor with radial distance r at constant axial position z.

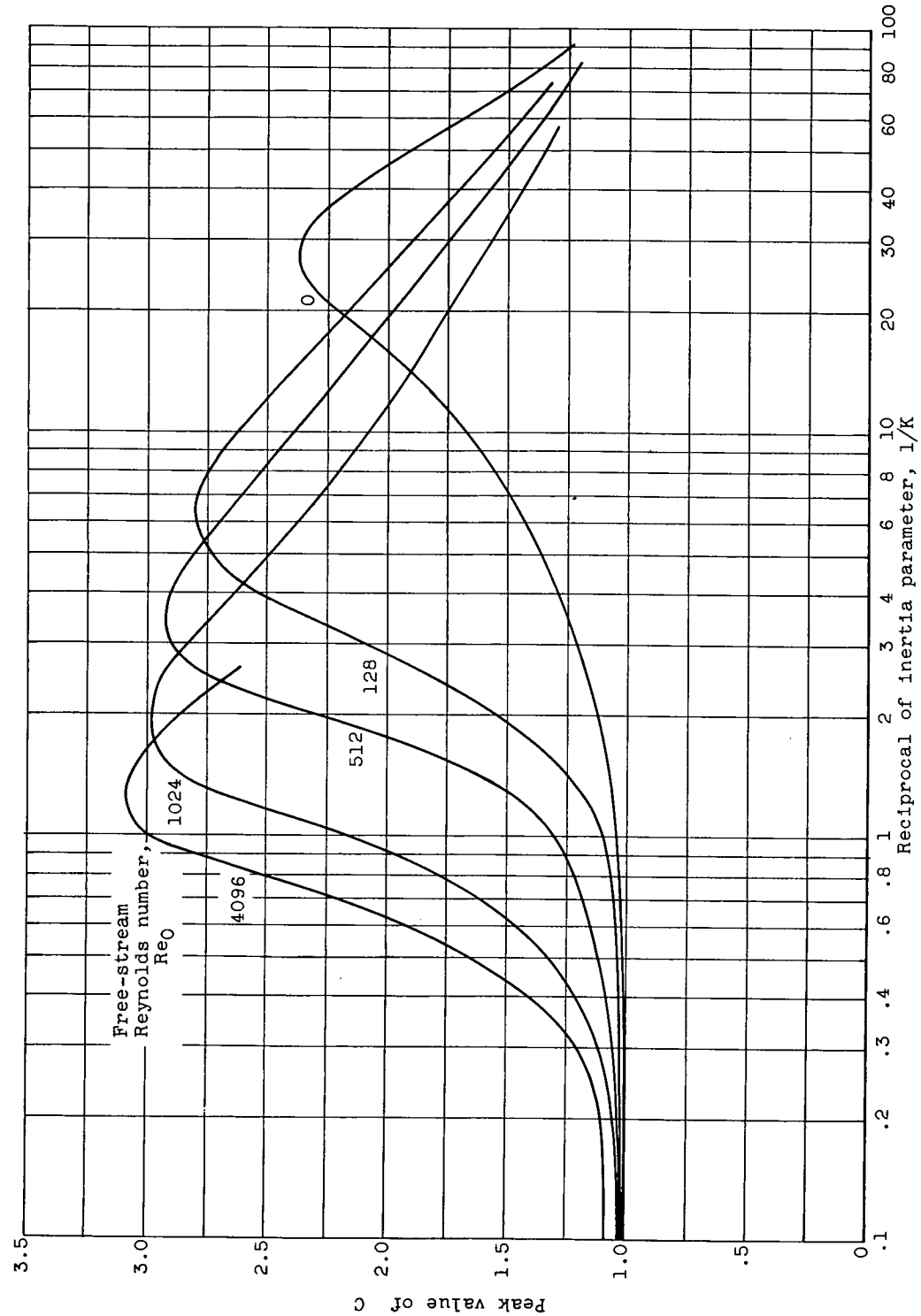

(a) z = 0.

Figure 6. - Variation of peak value of concentration factor with 1/K for constant free-stream Reynolds number.

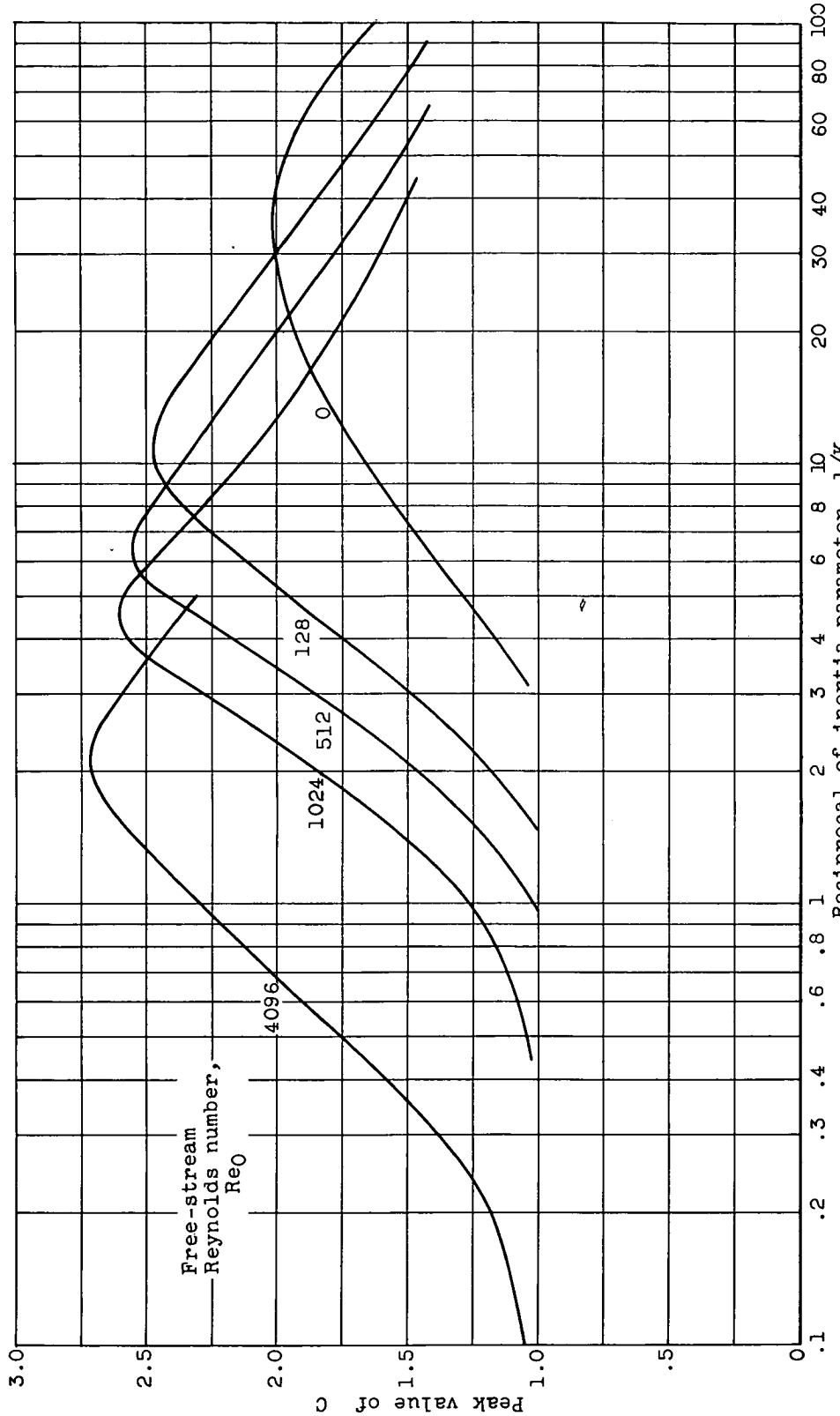

(b) z = -0.25.

Figure 6. - Concluded. Variation of peak value of concentration factor with 1/K for constant free-stream Reynolds number.

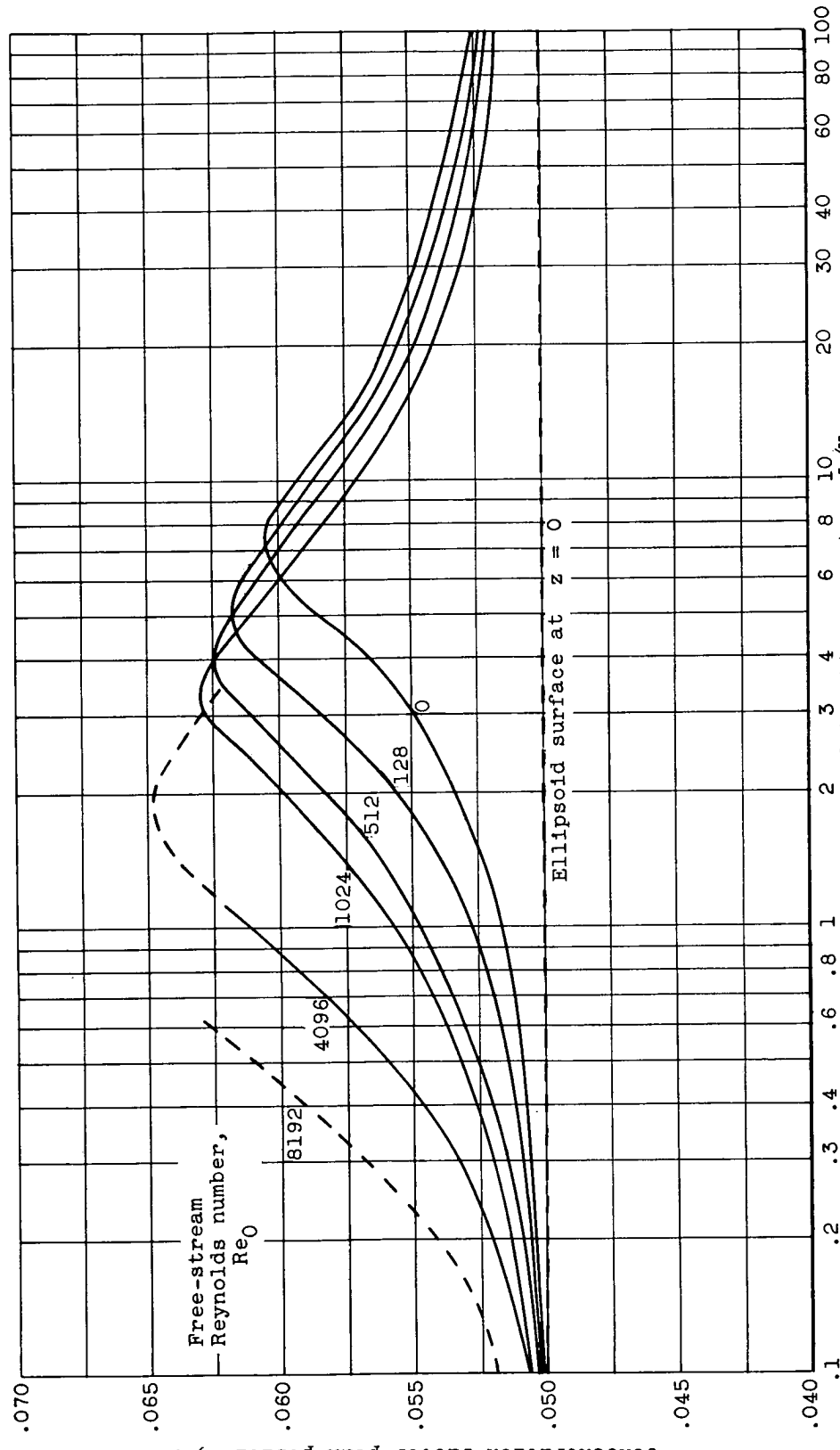

(a) z = 0.

Figure 7. - Variation of peak position of concentration factor with 1/K for constant free-stream Reynolds number.

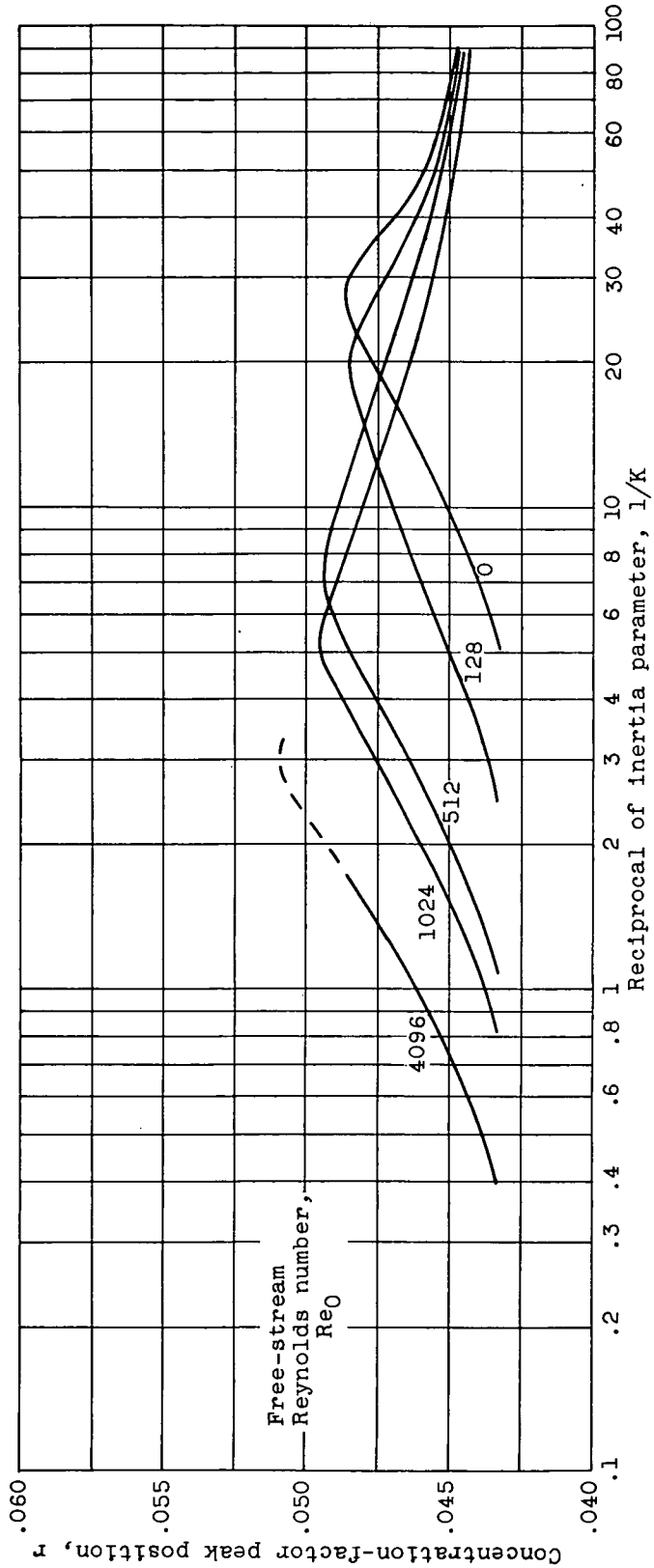

(b) z = -0.25.

Figure 7. - Concluded. Variation of peak position of concentration factor with 1/K for constant free-stream Reynolds number.

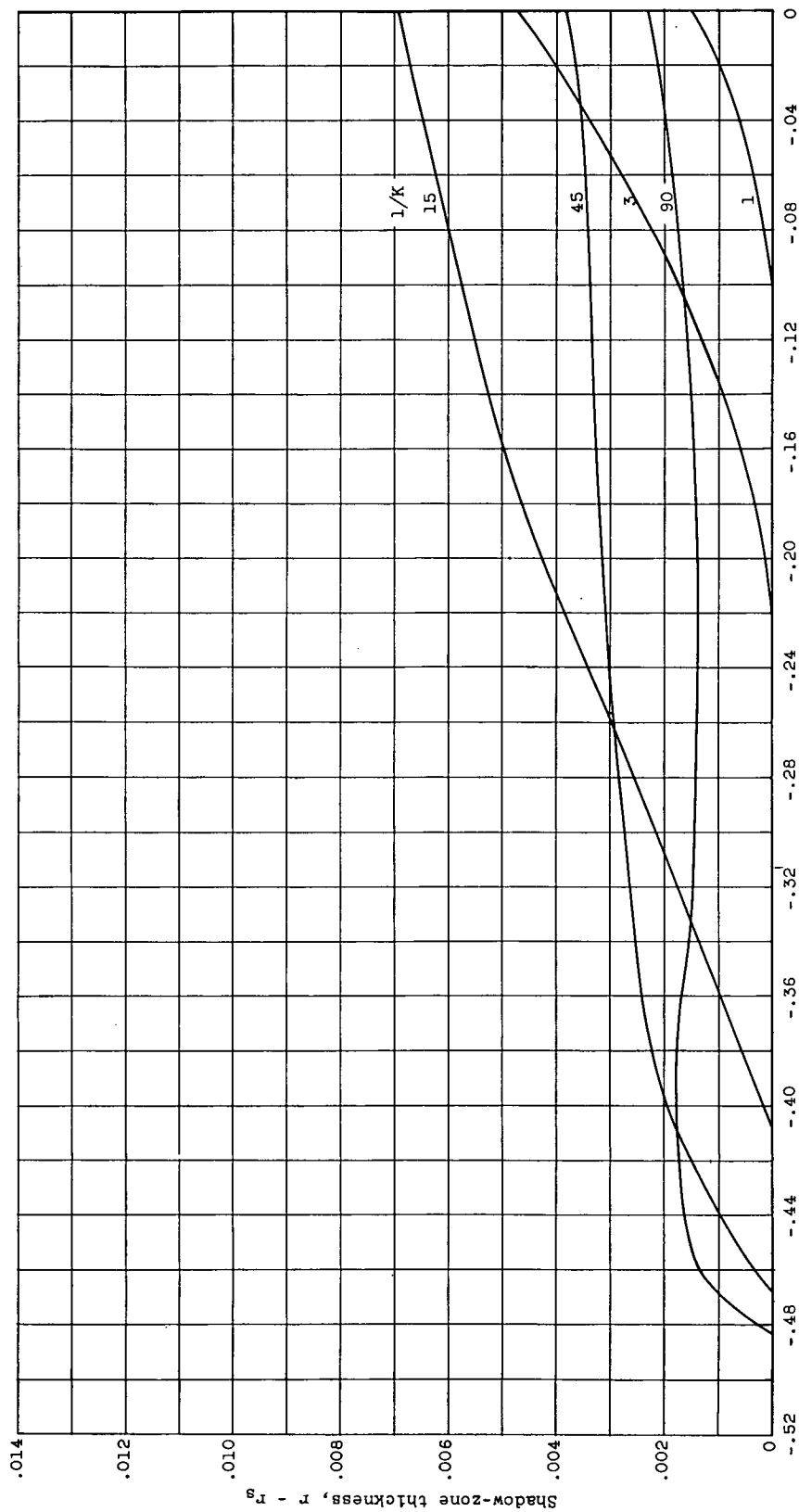

(a) Free-stream Reynolds number, 0.

Figure 8. - Thickness ($r - r_s$) of shadow zone as function of z-position.

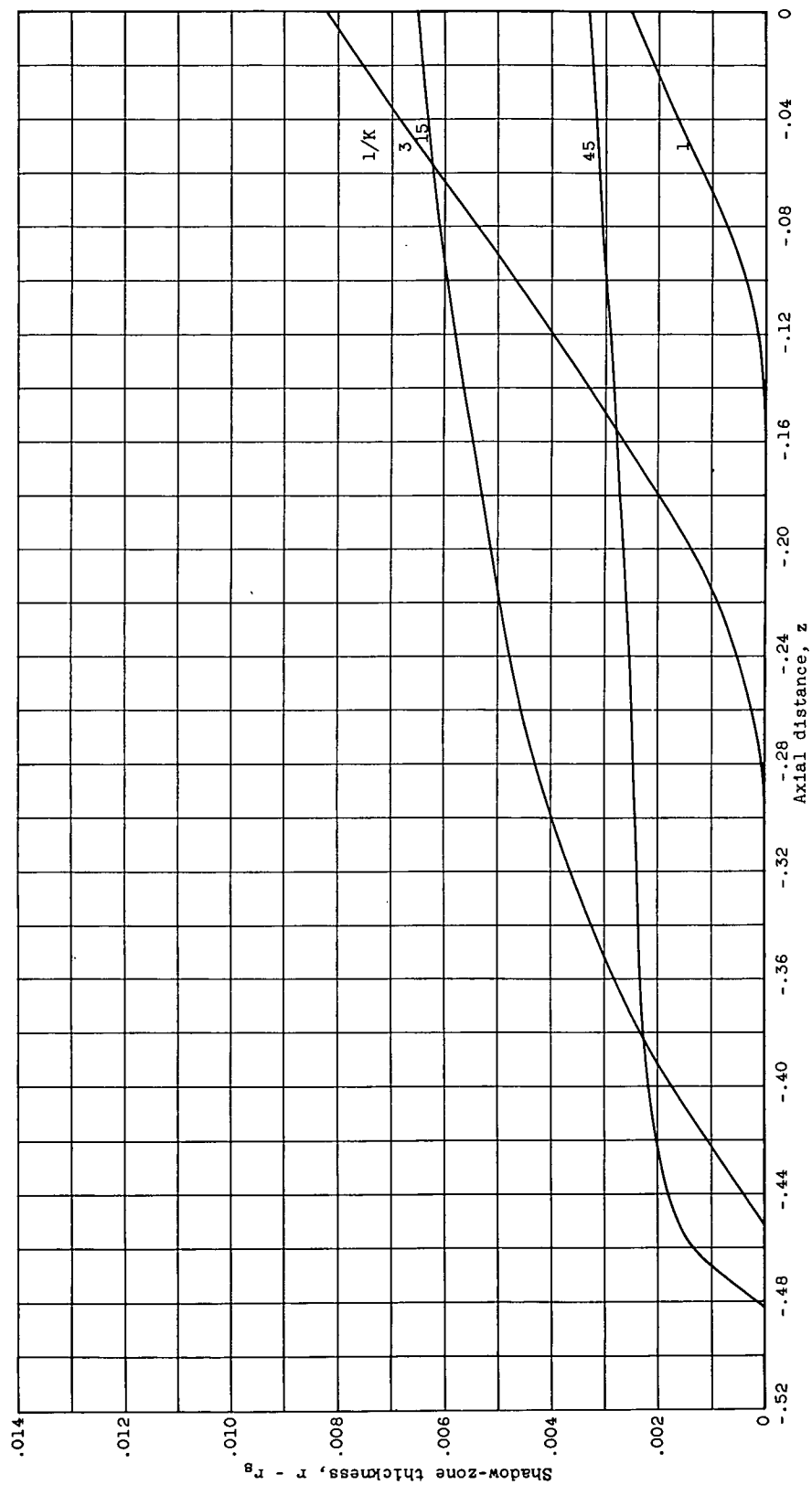

(b) Free-stream Reynolds number, 128.

Figure 8. - Continued. Thickness ($r - r_s$) of shadow zone as function of z-position.

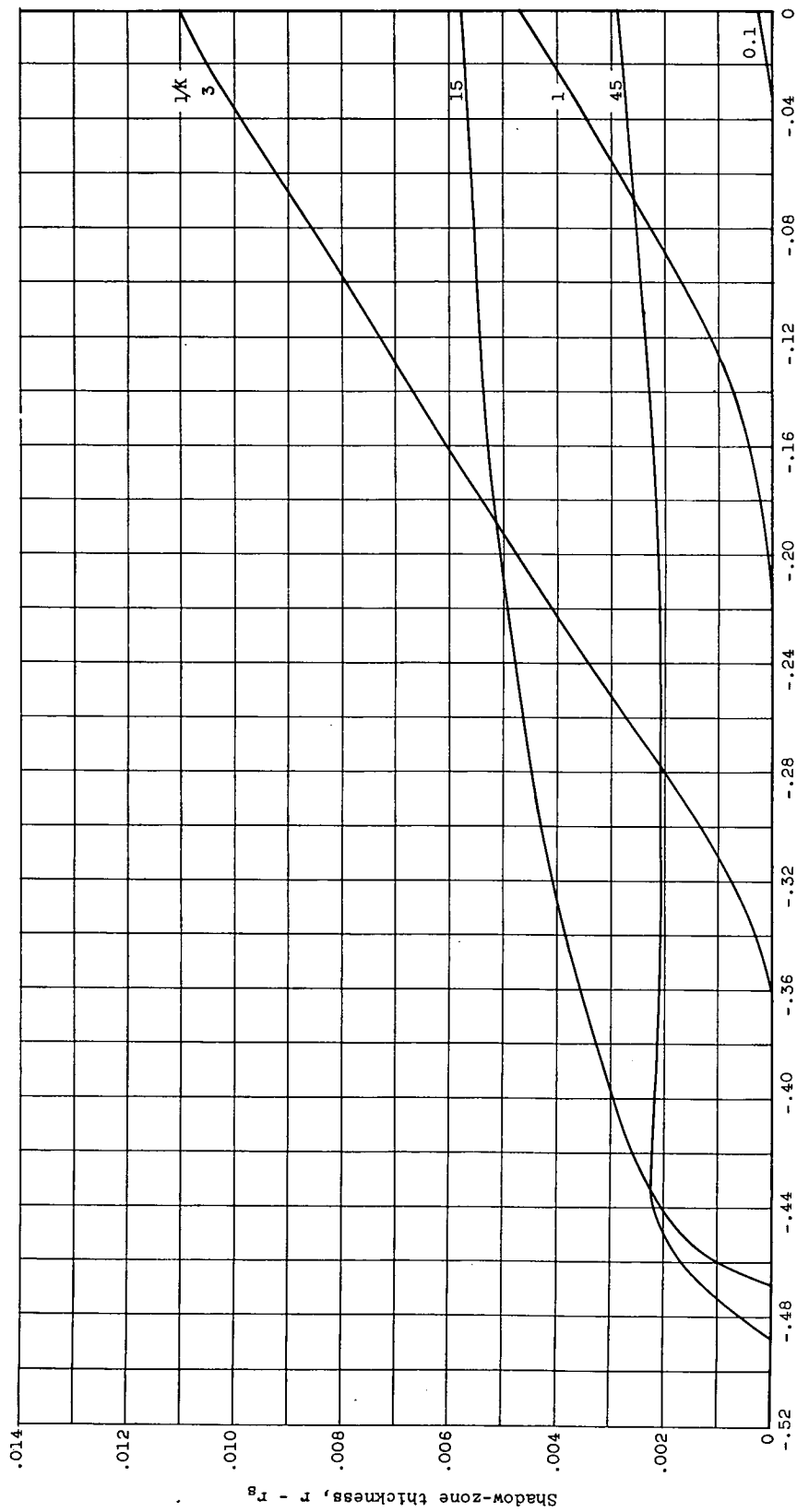

(c) Free-stream Reynolds number, 512.

Figure 8. - Continued. Thickness ($r - r_s$) of shadow zone as function of z-position.

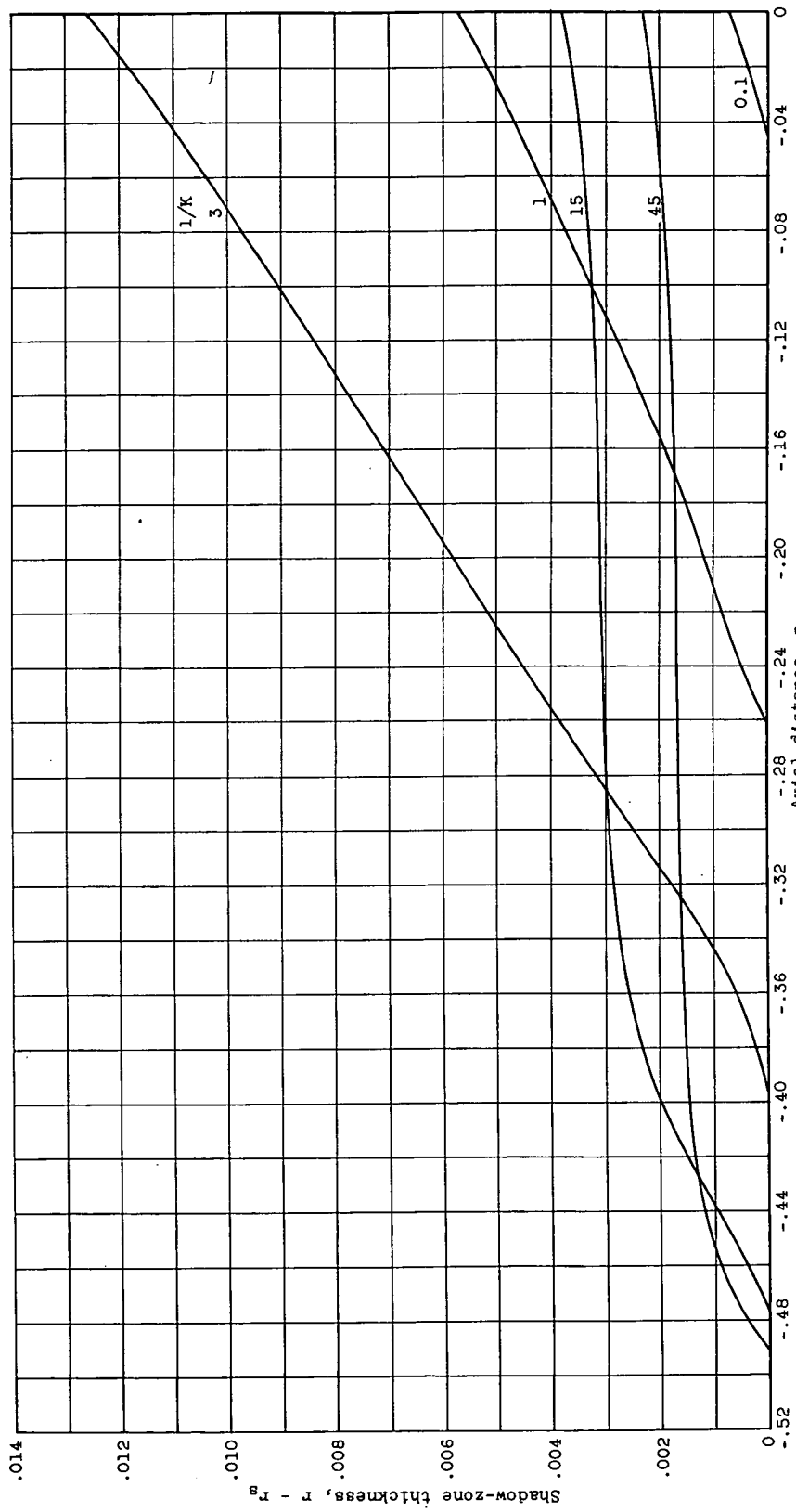

(d) Free-stream Reynolds number, 1024.

Figure 8. - Continued. Thickness (r - r_s) of shadow zone as function of z-position.

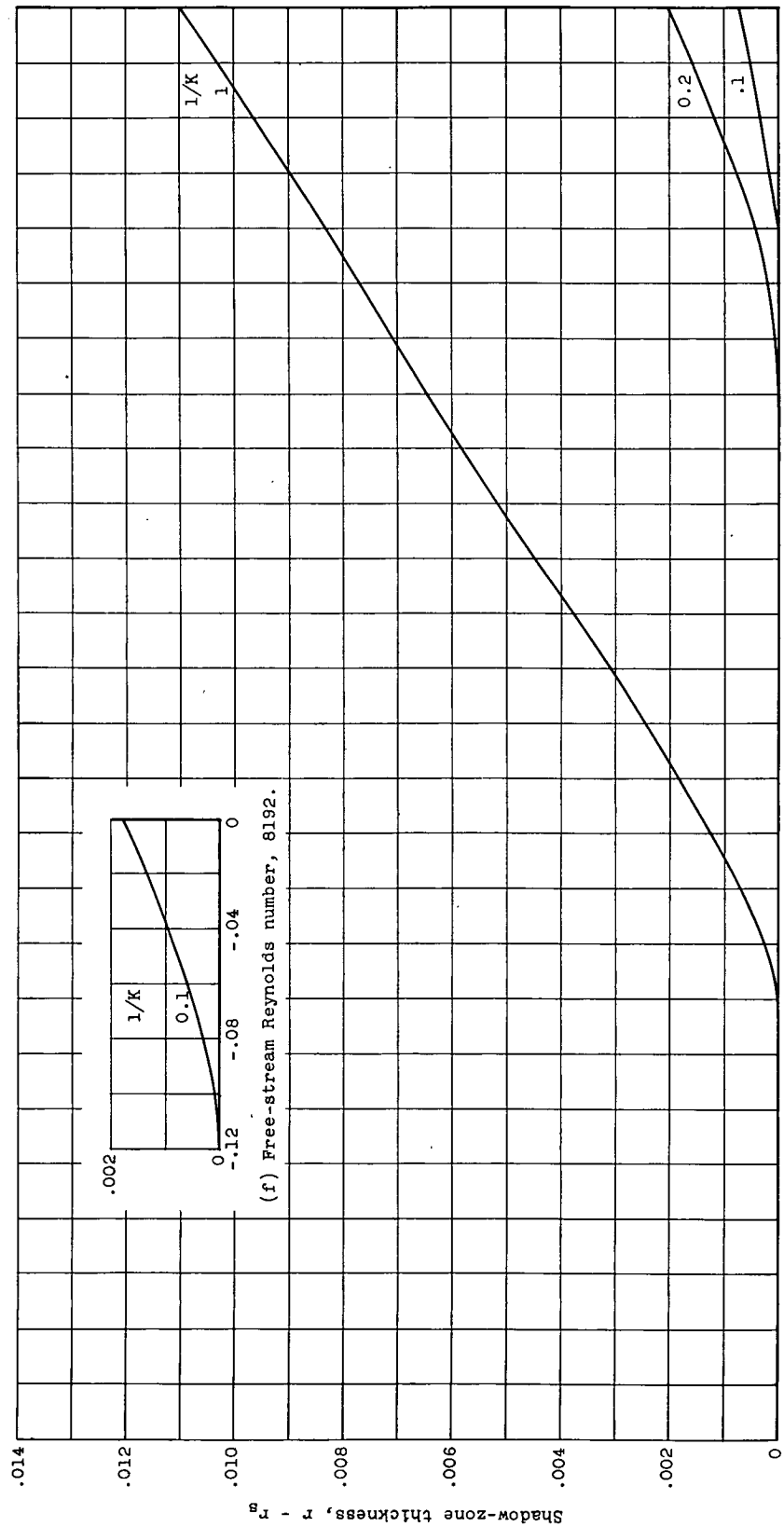

(e) Free-stream Reynolds number, 4096.

Figure 8. - Concluded. Thickness ($r - r_s$) of shadow zone as function of z-position.

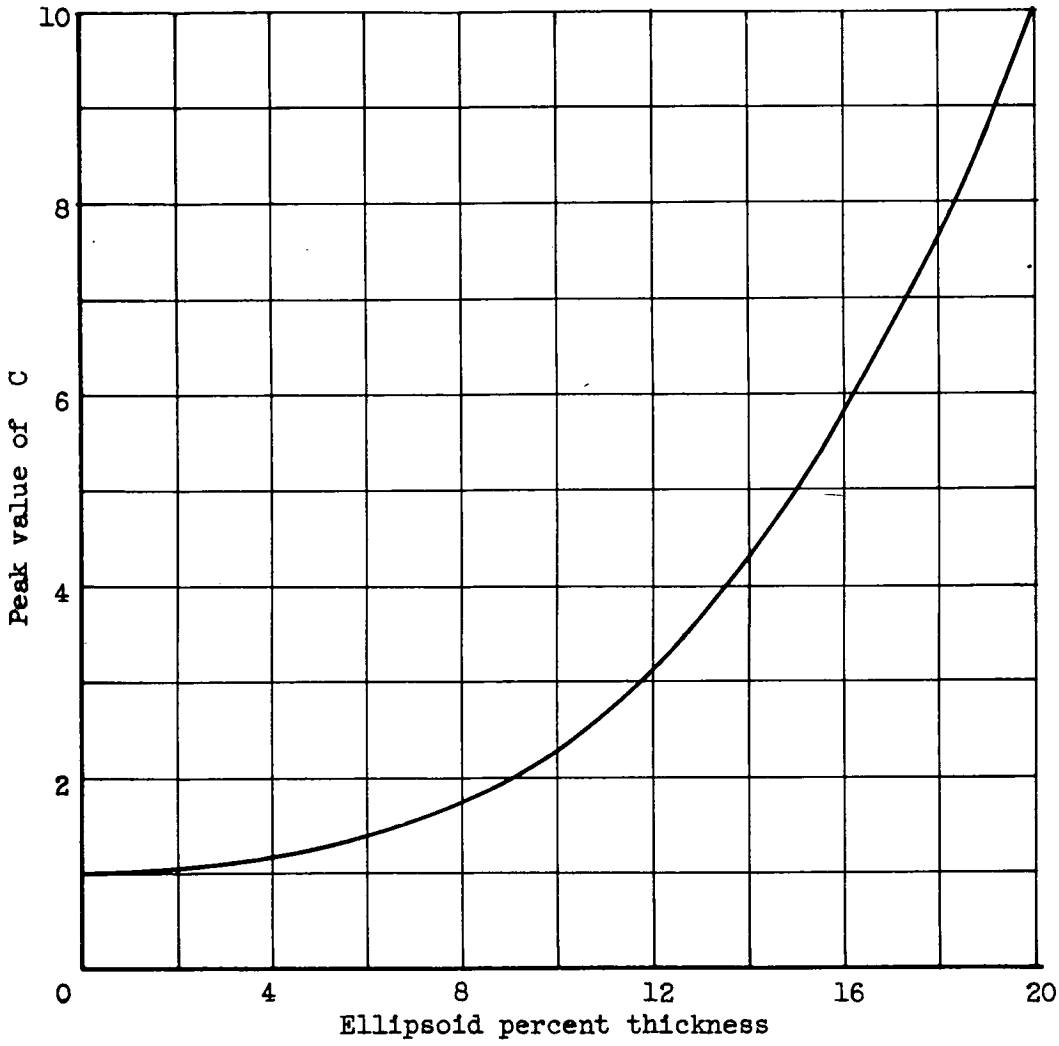

Figure 9. - Variation of peak value of concentration factor with ellipsoid thickness. Major axis, 10 feet; speed, 300 miles per hour; droplet diameter, 20 microns; altitude, 15,000 feet; Re_0, 1287; 1/K, 16.6; z = 0.

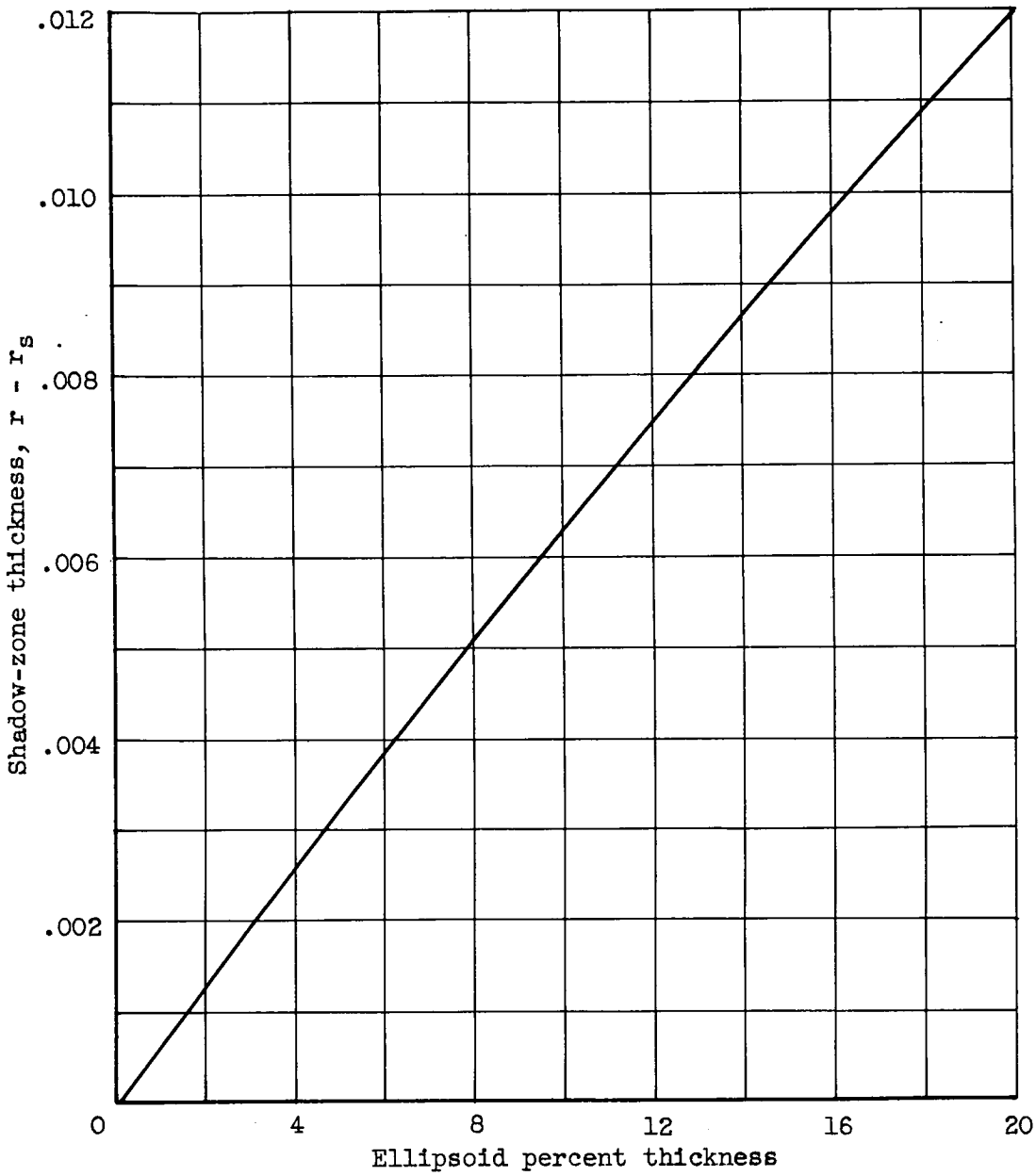

Figure 10. - Variation of shadow-zone thickness with ellipsoid thickness. Major axis, 10 feet; speed, 300 miles per hour; droplet diameter, 20 microns; altitude, 15,000 feet; Re_0, 1287; 1/K, 16.6; z = 0.

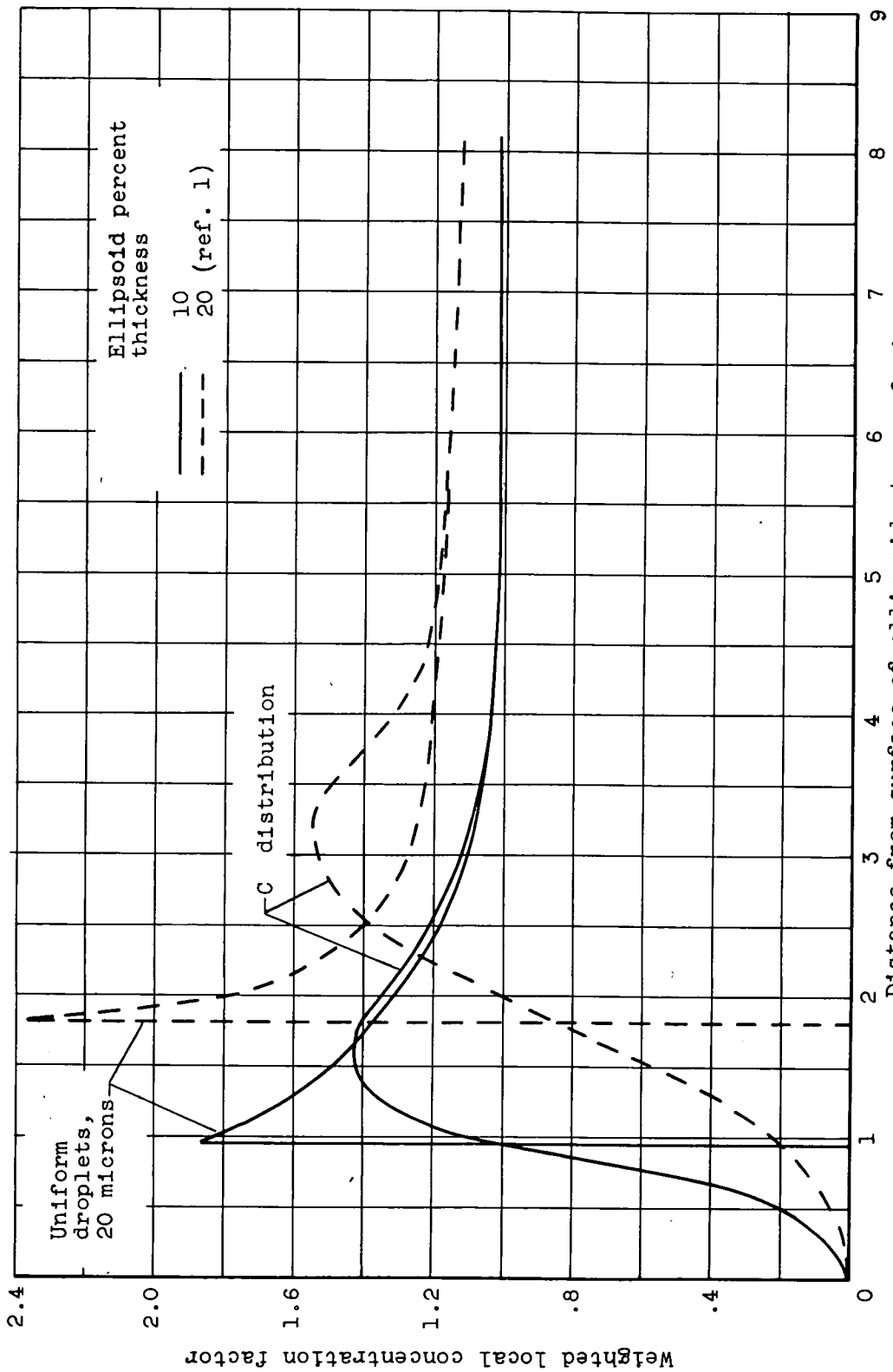

Figure 11. - Effect of droplet-size distribution on concentration factor for ellipsoid. Major axis length, 20 feet; velocity, 300 miles per hour; altitude, 15,000 feet; air temperature, 1° F; volume-median droplet diameter, 20 microns $Re_{0,med}$, 128.7; $1/K_{med}$, 33.1.